

023817-1-T

THE UNIVERSITY OF MICHIGAN

COLLEGE OF ENGINEERING

DEPARTMENT OF ELECTRICAL ENGINEERING & COMPUTER SCIENCE

Radiation Laboratory

MICROWAVE DIELECTRIC SPECTRUM OF ROCKS

F. T. Ulaby¹, T. Bengal¹, J. East¹, and M. C. Dobson¹

J. Garvin²

D. Evans³

¹The University of Michigan
Ann Arbor, MI 48109-2122

²NASA/Goddard Space Flight Center
Greenbelt, MD 20771

³Jet Propulsion Laboratory
Pasadena, CA 91109



NASA/GSFC Grant NAG-5-843 and
JPL Contract 947450

March, 1988

Ann Arbor, Michigan

{NASA-TM-89719} MICROWAVE DIELECTRIC
SPECTRUM OF ROCKS {NASA} 85 p CSCL 683

N88-19831

Unclas

G3/46 0130323

MICROWAVE DIELECTRIC SPECTRUM OF ROCKS

by

F. T. Ulaby¹, T. Bengal¹, J. East¹, and M. C. Dobson¹
J. Garvin²
D. Evans³

¹The University of Michigan
Ann Arbor, MI 48109-2122

²NASA/Goddard Space Flight Center
Greenbelt, MD 20771

³Jet Propulsion Laboratory
Pasadena, CA 91109

March, 1988

Supported by:

NASA/GSFC Grant NAG-5-843 and
JPL Contract 947450

TABLE OF CONTENTS

	<u>Page</u>
ABSTRACT.....	iii
1. INTRODUCTION.....	1
2. DIELECTRIC PROBE MEASUREMENT TECHNIQUE.....	2
2.1 Third-Order Equivalent Circuit.....	3
2.2 First-Order Equivalent Circuit.....	11
2.2.1 Reflection Measurement Technique.....	11
2.2.2 Group-Delay Measurement Technique.....	12
2.3 Sample Preparation For Permittivity Measurement.....	14
2.4 Measurement Accuracy and Precision.....	15
3. RESONANT-CAVITY PERTURBATION TECHNIQUE.....	20
3.1 Measurement Accuracy and Precision.....	25
3.2 Cavity Characteristics.....	27
3.3 Effects of Surficial Water.....	27
4. MEASURED DATA.....	33
5. ANALYSIS OF PERMITTIVITY DATA.....	33
5.1 Distribution of Measured Data.....	33
5.2 Dependence on Density.....	39
5.3 Dependence on Mineral Composition.....	45
5.3.1 Igneous Volcanic Silicates.....	45
5.3.2 Igneous Plutonic Silicates.....	45
5.3.3 Igneous Silicates.....	50
5.3.4 Sedimentary Silicates.....	50
5.3.5 All Silicates.....	57
6. ANALYSIS OF DIELECTRIC-LOSS DATA.....	57
6.1 Frequency Variation.....	57
6.2 Dependence on Density.....	66
6.3 Dependence on Mineral Composition.....	66
7. CONCLUSIONS.....	66
REFERENCES.....	80

ABSTRACT

A combination of several measurement techniques was used to investigate the dielectric properties of 80 rock samples in the microwave region. The real part of the dielectric constant, ϵ' , was measured in 0.1 GHz steps from 0.5 GHz to 18 GHz, and the imaginary part, ϵ'' , was measured at five frequencies extending between 1.6 GHz and 16 GHz. In addition to the dielectric measurements, the bulk density was measured for all the samples and the bulk chemical composition was determined for 56 of the samples. This study shows that ϵ' is frequency-independent over the 0.5-18 GHz for all rock samples, and that the bulk density ρ accounts for about 50% of the observed variance of ϵ' . For individual rock types (by genesis), about 90% of the observed variance may be explained by the combination of density and the fractional contents of SiO_2 , Fe_2O_3 , MgO , and TiO_2 . For the loss factor ϵ'' , it was not possible to establish statistically significant relationships between it and the measured properties of the rock samples (density and chemical composition).

PRECEDING PAGE BLANK NOT FILMED

1. INTRODUCTION

The purpose of this study is to investigate the microwave dielectric properties of igneous and sedimentary rocks, in support of radar investigations of the Earth's geology and of the proposed Mars Orbiting Radar and Radiometer (MORAR) mission to Mars.

Several studies have been reported in the literature on the dielectric properties of rocks [1-6], but in most of these studies the reported experimental measurements had been made either at MHz or lower frequencies, or at one or very few microwave frequencies. Thus, no continuous microwave spectra of the relative dielectric constant ϵ have been reported to date. Furthermore, the majority of the reported data for the dielectric loss factor ϵ'' is of questionable accuracy. This is because ϵ'' of most rocks is between 0.01 and 0.1, and most dielectric measurement techniques do not have the accuracy required for measuring values that small.

The relative dielectric constant ϵ of a material is defined as

$$\epsilon = \epsilon' - j\epsilon'' ,$$

where the real part ϵ' is the permittivity of the material (relative to that of free space)

and the imaginary part ϵ'' is its dielectric loss factor (also relative to ϵ_0 of free space).

This study focuses on the spectral region extending from 0.5 GHz to 18 GHz. A combination of several measurement techniques was used to measure ϵ over this frequency range. It included two probe techniques for measuring ϵ' in steps of 0.1 GHz from 0.5 GHz to 18 GHz, and a resonant cavity perturbation technique for measuring ϵ''

at five frequencies extending from 1.6 GHz to 16 GHz. As discussed later, because these cavity measurements are very time-consuming, it was not possible to make the measurements at more than five frequencies (within the constraints of available resources) without compromising measurement accuracy.

The dielectric data reported in this study were generated from measurements performed for 80 rock samples. Each data point represents the average of several measurements corresponding to spatially different parts of the rock sample. The variability among measurements made for a given rock sample is an indicator of the sample's spatial inhomogeneity. Such variations may be due to density variations or variations in chemical composition among mineral constituents. In addition to measuring the dielectric behavior of each sample, its density and bulk chemical composition were measured and documented also.

This report provides listings of the measured data, analyses of the associated measurement accuracies, and analyses relating ϵ' and ϵ'' to the density ρ of the measured samples and to their chemical contents.

2. DIELECTRIC PROBE MEASUREMENT TECHNIQUE

The permittivity data reported in this study are based on measurements of the complex reflection coefficient of a coaxial probe terminated in the material under test. Two techniques were used. The first one is based on a third-order equivalent circuit that can be used for measuring the dielectric constant of any rock sample across the full frequency range of interest (0.5 - 18 GHz). The second one is a simpler first-order

equivalent circuit, but its validity range is limited to frequencies below 10 GHz if ϵ' is larger than 8. For all rock samples investigated in this study, ϵ' was found to be approximately independent of frequency over the 0.5-18 GHz range. Because it is simpler to use and calibrate, the first-order technique was initially used to measure ϵ' of a given sample, and if ϵ' was found to exceed 8 over the 0.5-10 GHz range, the sample was remeasured using the more exact third-order technique. Brief descriptions of these two techniques are given next.

2.1 Third-Order Equivalent Circuit

The dielectric probe system (Fig. 1) consists of a swept RF source, a network analyzer (HP 8510A), and associated couplers and data processing instrumentation. Fig. 2(a) shows a cross section of the probe tip and the dimensions of two of the probes examined in this study. The operation of open-ended coaxial lines to measure the dielectric constant of unknown materials is well-documented in the literature [7]-[9].

The input reflection coefficient at the prober tip ρ is given by

$$\rho = \frac{Z_L - Z_0}{Z_L + Z_0} = \frac{Y_0 - Y_L}{Y_0 + Y_L}, \quad (1)$$

where $Y = 1/Z$, Z_0 is the line impedance, and Z_L is the load impedance, which is governed by the geometry of the probe tip and the dielectric constant of the material it is in contact with or immersed in (for liquid materials). In general, an open-ended

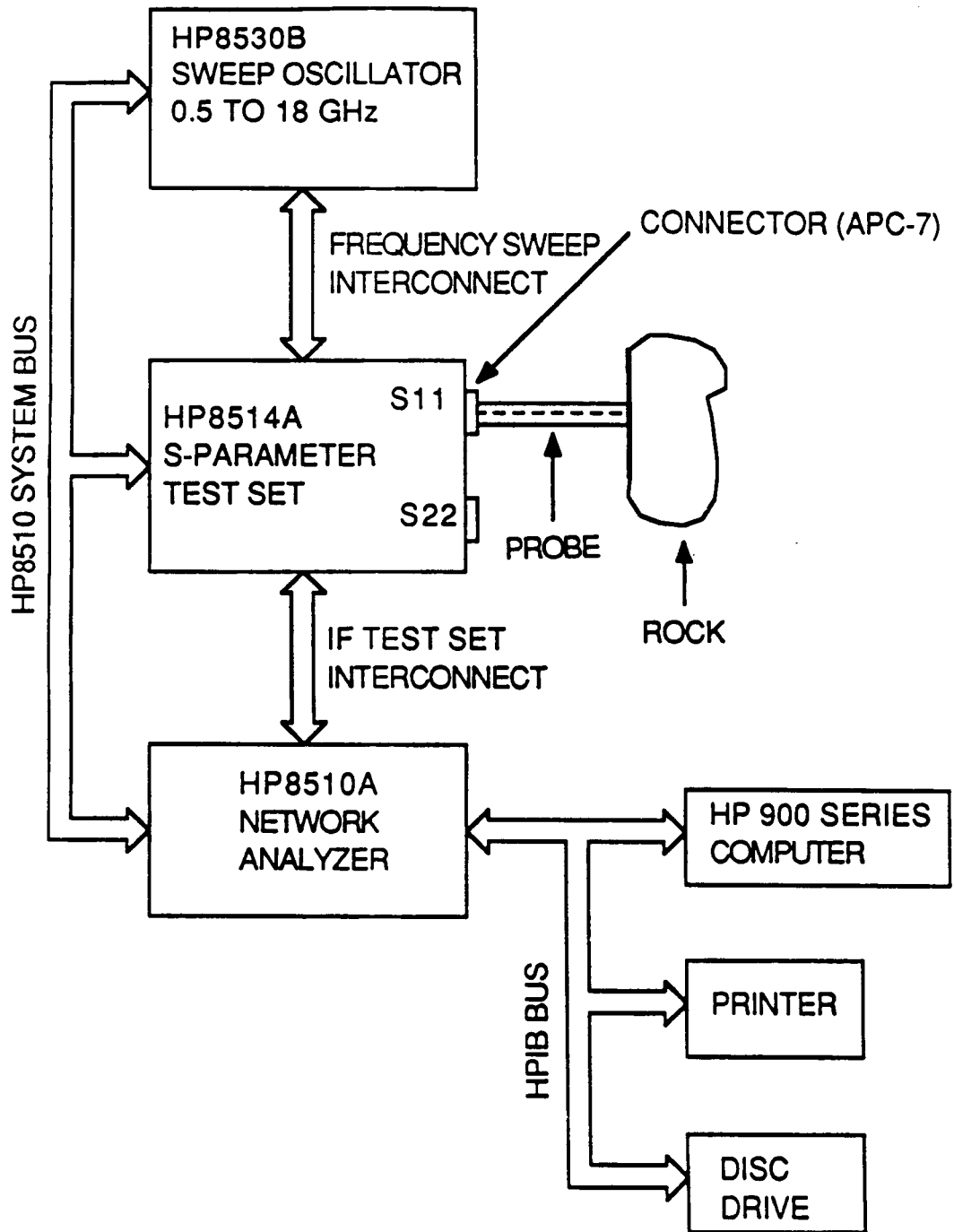
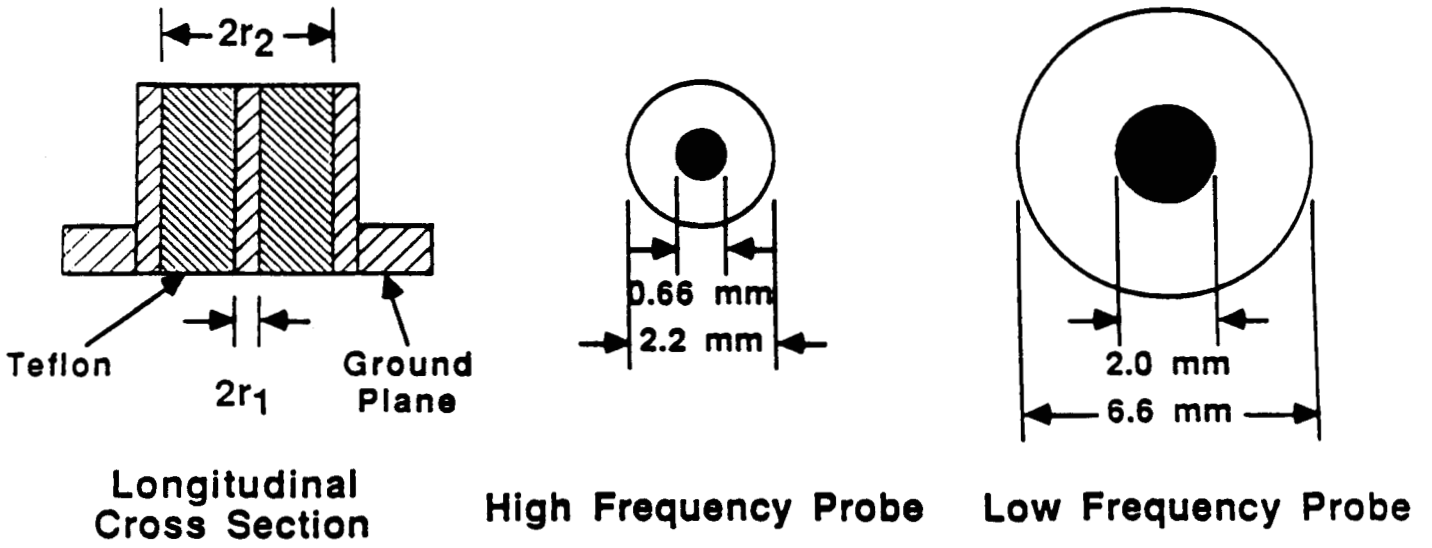
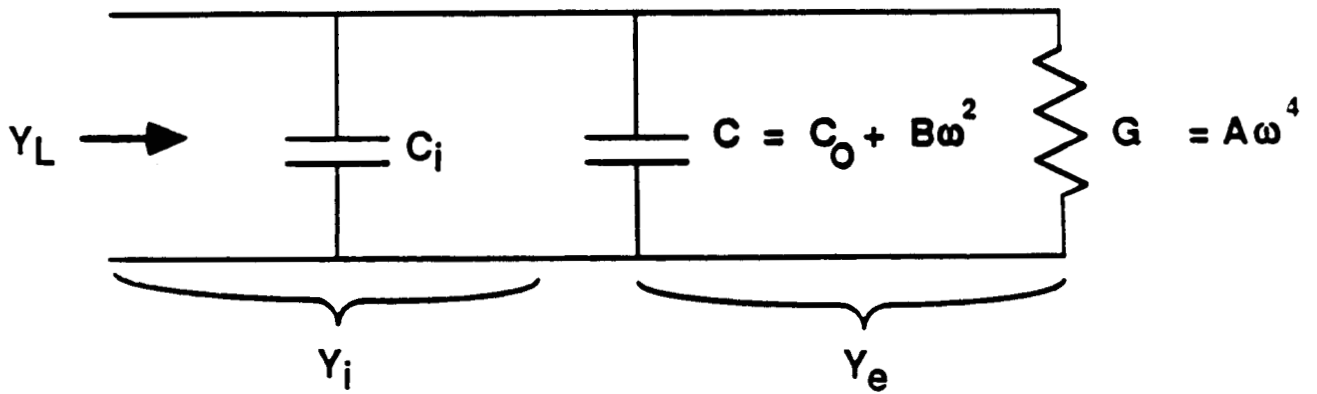


Fig. 1. Block diagram of the dielectric-probe measurement system.



(a) Dielectric Probes



(b) Probe Equivalent Circuit

Fig. 2. The dielectric probe; (a) cross-sectional views, and (b) equivalent circuit.

coaxial line may be described by an equivalent circuit of the form shown in Fig. 2(b). When placed in contact with a homogeneous material whose thickness is sufficient to simulate a slab of infinite electrical thickness, an open coaxial line has an admittance $Y_L(\omega, \epsilon)$ given by

$$Y_L(\omega, \epsilon) = Y_i(\omega) + Y_e(\omega, \epsilon) , \quad (2)$$

where $Y_i(\omega) = j\omega C_i$ is the "internal" admittance corresponding to the fringing capacitance C_i that accounts for the fringing field in the Teflon region between the inner and outer conductors of the line. The "external" admittance Y_e , which is a function of both ω and the complex dielectric constant ϵ of the material under test, consists of a frequency-dependent capacitor $C(\omega, \epsilon)$ in parallel with a radiation conductance $G(\omega, \epsilon)$

$$Y_e(\omega, \epsilon) = j\omega C(\omega, \epsilon) + G(\omega, \epsilon) . \quad (3)$$

The capacitor $C(\omega, \epsilon)$ represents the fringing field concentration in the dielectric medium (ϵ) surrounding the probe tip, and the conductance $G(\omega, \epsilon)$ represents the radiation into the dielectric medium.

When the medium surrounding the probe tip is free space (i.e., an open-ended line), these two equivalent-circuit elements vary according to

$$C(\omega, \epsilon_0) = C_0 + B\omega^2 \quad (4)$$

$$G(\omega, \epsilon_0) = A\omega^4, \quad (5)$$

where C_0 , B , and A are constants for a given probe-tip geometry. If the radial dimensions of the coaxial line (namely, r_1 and r_2) are small compared to the wavelength λ , computations using the expressions given in Marcuvitz [10] yield values for A and B that are sufficiently small that the external admittance may be approximated as $Y_e(\omega, \epsilon_0) \cong j\omega C_0$. If the dielectric constant of the medium surrounding the probe tip is not the free space value ϵ_0 , however, the above simplification may lead to unacceptably large errors. Hence, in the general case we have

$$Y_e(\omega, \epsilon) = j\omega(C_0 + B\omega^2) + A\omega^4. \quad (6)$$

According to the theorem developed by Deschamps [11], the input admittance of an antenna immersed in a medium of complex dielectric constant ϵ is related to the input admittance in free space through

$$Y_e(\omega, \epsilon) = \sqrt{\frac{\epsilon}{\epsilon_0}} Y_e\left(\omega \sqrt{\frac{\epsilon}{\epsilon_0}}, \epsilon_0\right). \quad (7)$$

The above expression is for materials characterized by $\mu = \mu_0$. If we regard the open-ended coaxial line as an antenna and henceforth abbreviate the relative dielectric constant ratio ϵ/ϵ_0 as simply ϵ , we can write the following expression for the

total input admittance of the probe when placed in contact with a material of relative dielectric constant ϵ :

$$Y_L(\omega, \epsilon) = j\omega C_i + j\omega C_0 \epsilon + jB\omega^3 \epsilon^2 + A\omega^4 \epsilon^{2.5} . \quad (8)$$

With the line admittance Y_0 known, measurements of the amplitude and phase of ρ by the network analyzer system (Fig. 1) lead to a measurement of Y_L . The next step is to determine ϵ from Y_L . This is accomplished by 1) calibrating the measurement probe in order to establish the values of the constants C_i , C_0 , B , and A , and 2) developing an iterative program for finding a value for ϵ that minimizes the error between the measured value of Y_L and the value calculated from the expression on the right-hand side of (8).

A. Usable Frequency Range

The radii r_1 and r_2 of the coaxial line govern three important characteristics of the dielectric measurement system:

1) The ratio r_1/r_2 determines the characteristic impedance Z_0 of the line. For 50- Ω Teflon-filled lines, this ratio is approximately 0.3.

2) The difference $(r_2 - r_1)$ determines the cutoff wavelength of the TM modes [10, p. 74]; the cutoff wavelength of the TM_{01} modes is $\lambda_c \cong 2(r_2 - r_1)$. Table 1

Table 1. Dimensions and cutoff wavelength λ_c for the TM_{01} mode for four standard-size coaxial cables.

Cable	Type	r_2 (mm)	r_1 (mm)	r_2/r_1	λ_c (mm)
0.09"	Teflon	0.84	0.26	3.28	1.18
0.14"	Teflon	1.50	0.46	3.30	2.13
0.25"	Teflon	2.66	0.82	3.22	3.76
0.35"	Teflon	3.62	1.12	3.22	5.07

provides a list of the dimensions and cutoff wavelengths of four standard coaxial lines used in this study. For a medium with a complex dielectric constant $\epsilon = \epsilon' - j\epsilon''$, the wavelength in the medium λ_ϵ is related to the wavelength in free space λ_0 by

$$\lambda_\epsilon = \lambda_0 \left[\frac{\epsilon'}{2} (1 + \sec \delta) \right]^{-1/2}, \quad (9)$$

where $\delta = \tan^{-1} (\epsilon''/\epsilon')$. To avoid the propagation of TM modes, the condition $\lambda_\epsilon < \lambda_c$ should be satisfied. Because most rocks are low-loss materials and ϵ' seldom exceeds 10, all of the probes listed in Table 1 are appropriate for measuring ϵ' of rocks at frequencies below 20 GHz. In this investigation 0.14-in probes were used exclusively.

B. Calibration

Calibration entails finding the values of the constants C_i , C_0 , B , and A of (8) for each probe used in this study. Under ideal circumstances, one needs to determine these constants only once and at only one frequency. The equivalent-circuit model, however, is only approximate; hence, it is necessary to determine these constants at each frequency that the probe is intended to be used. For example, it was found that the *constant A* varies approximately at $1/\omega$, which means that the conductance term $G(\omega)$ varies as ω^3 , not ω^4 .

Each dielectric probe was calibrated by measuring the complex reflection

coefficient under four termination conditions: 1) short circuit, 2) open circuit, 3) probe immersed in distilled water, and 4) probe immersed in methanol. Distilled water and methanol were used because their dispersion spectra are well known [12], [13].

2.2 First-Order Equivalent Circuit

If the diameter of the coaxial probe is much smaller than the wavelength in the material under test, λ_e , the equivalent-circuit admittance Y_e simplifies to only one term, $j\omega C_0\epsilon$, because the other two terms become negligibly small. For the 0.14-in probe used in this study, the condition

$$f(\text{GHz}) \leq 50 / \sqrt{\epsilon'} , \quad (10)$$

must be satisfied in order for the first-order model to yield accurate results. This condition was found by comparing measurements made with this technique to measurements made using the more-exact technique described in the previous section.

2.2.1 Reflection Measurement Technique

For the first-order equivalent circuit, the admittance,

$$Y_L(\omega, \epsilon) \equiv j\omega C_i + j\omega C_0 \epsilon , \quad (11)$$

can be determined by measuring the reflection coefficient ρ . The constants C_i and

C_0 can be determined by measuring $Y_L(\omega, \epsilon)$ for two materials with known ϵ . With the constants known, ϵ of an unknown material may be computed directly from

$$\epsilon = \frac{1}{C_0} \left[\frac{Y_0}{j\omega} \left(\frac{1-\rho}{1+\rho} \right) - C_i \right], \quad (12)$$

by measuring ρ . The coaxial line is a standard 50-ohm line (i.e., $Y_0 = 1/50$).

2.2.2 Group-Delay Measurement Technique

As an alternative to measuring ρ in order to determine ϵ , a group-delay technique was developed which requires calibration against only one calibration material rather than two. For low loss materials with $\epsilon'' \ll \epsilon'$,

$$Y_L \cong j\omega (C_i + \epsilon' C_0), \quad (13)$$

and the reflection coefficient

$$\begin{aligned} \rho &= |\rho| e^{j\phi} \\ &= \frac{Y_0 - Y_L}{Y_0 + Y_L} \end{aligned} \quad (14)$$

has a phase angle given by

$$\phi = 2 \cot^{-1} [50 \omega (C_i + \epsilon' C_0)]. \quad (15)$$

For the 0.141-in probe, the constants C_i and C_0 are on the order of 0.02 picofarads.

Consequently, the entire quantity inside the square brackets is much smaller than 1 if

$\omega \leq 2\pi \times 20$ GHz and $\epsilon' \leq 10$. Hence, $\cot^{-1}(\quad)$ may be expanded in a Taylor series

$$\cot^{-1}(x) = \pi/2 - x + x^3/3 - \dots, \quad (16)$$

and if we retain only the first two terms, we have

$$\phi \cong \pi - 100 \omega (C_i + \epsilon' C_0) . \quad (17)$$

The group delay τ is defined as the change in the phase of ρ as a function of frequency,

$$\tau = \frac{\partial \phi}{\partial \omega} = -100 (C_i + \epsilon' C_0) . \quad (18)$$

If the group delay is measured with the probe in air (with $\epsilon' = 1$) and not in contact with any other material, we get the reference group delay τ_0 ,

$$\tau_0 = -100 (C_i + C_0) . \quad (19)$$

The differential group delay is defined as

$$\begin{aligned} \Delta \tau &= \tau - \tau_0 \\ &= -100 C_0 (\epsilon' - 1) , \end{aligned} \quad (20)$$

from which we obtain the expression

$$\epsilon' = 1 - \frac{\Delta\tau}{100 C_0} . \quad (21)$$

The constant C_0 may be determined by measuring $\Delta\tau$ for one material of known ϵ' .

The group delay τ and τ_0 can be measured directly by the HP 8510A network analyzer.

Comparison of results using the group-delay technique with results obtained using the more-exact reflection coefficient technique has led to the conclusion that the condition

$$f \text{ (GHz)} \leq 30 / \sqrt{\epsilon'} , \quad (22)$$

should be satisfied in order for the approximation made in going from (16) to (17) to be valid.

2.3 Sample Preparation For Permittivity Measurements

When using the coaxial probe to measure the permittivity of a solid material, the following two conditions must be satisfied (in order for the measurements to produce accurate results):

- (1) The thickness of the sample must be at least equal to the probe diameter.

For the 0.14-in probe, this condition is satisfied if the thickness is greater than 4 mm.

(2) The surface of the sample in contact with the probe must be very smooth in order to insure good electrical contact. This was achieved by having each rock sample cut with a rock saw to obtain a flat surface and then the surface was smoothed using a table-top rotary sander.

To avoid dielectric effects that may be caused by the possible presence of surficial water molecules on the sample, each sample was dried in an oven for 15 minutes at 100°C prior to performing the dielectric measurements. It was found, however, that there was very little difference, if any, between the results obtained after drying the samples and those obtained on the basis of the measurements made prior to drying the samples. An entirely different conclusion was reached for the measurements of the dielectric loss factor ϵ'' ; for some rocks, the values measured prior to drying the sample were as much as twice the values measured for the samples dry (Section 3.3).

2.4 Measurement Accuracy and Precision

The measurement accuracy of the probe technique was evaluated by comparing the permittivity measured by the probe with the permittivity of standard materials. The reference materials are homogeneous, thick blocks of solid materials, such as teflon, whose dielectric constants had been carefully measured using waveguide techniques. A typical comparison is shown in Fig. 3 for a material with $\epsilon' = 8.0$. Based on this and other comparisons, we estimate the probe measurement accuracy to be better than ± 0.03 of the measured value.

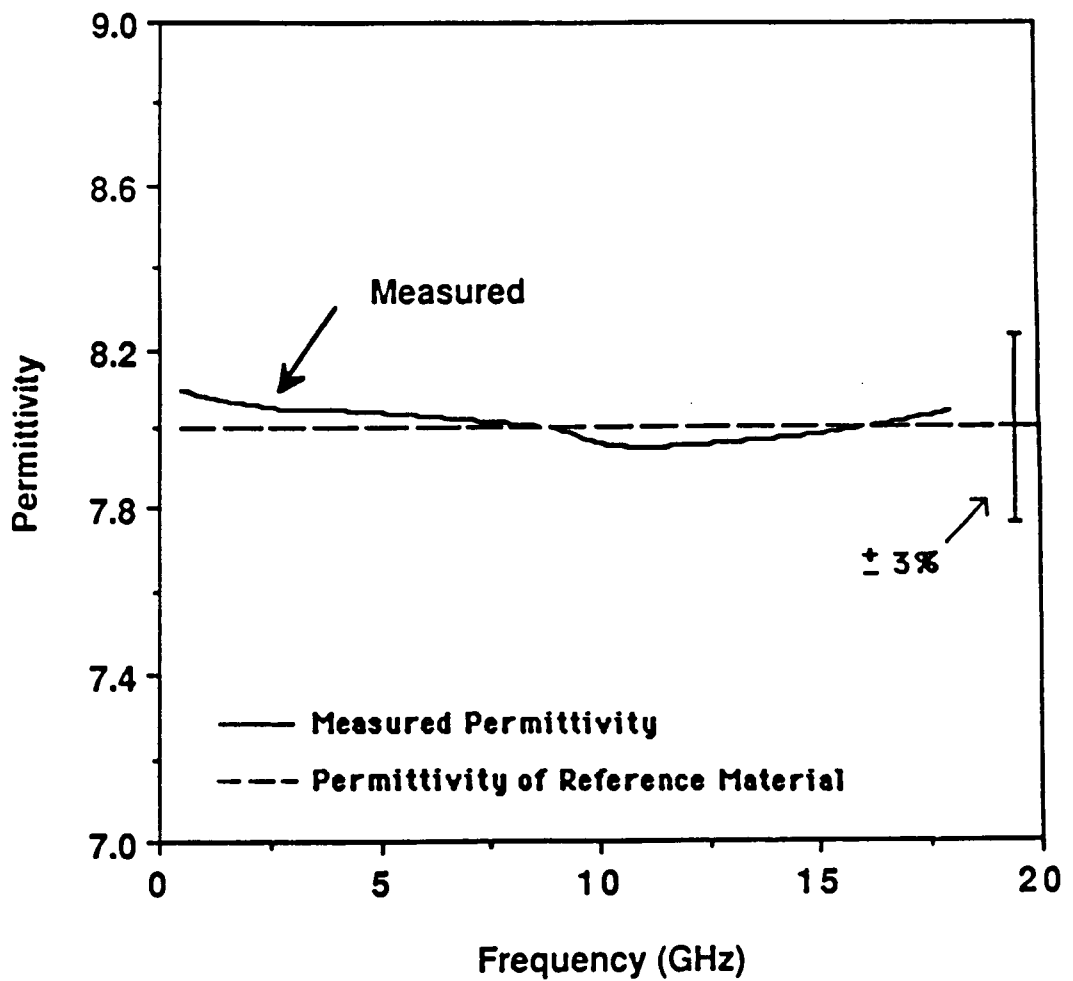


Fig. 3. Comparison of the measured permittivity with the permittivity of a reference material.

By accuracy, we refer to the absolute level of ϵ' , whereas by precision, we refer to the variability associated with the spatial inhomogeneity of the sample. For all rock samples, ϵ' was measured by applying the probe at at-least 16 spatially different locations on the polished surface of the rock sample. In each case, we computed the mean value of ϵ' , the associated standard deviation S , and the ratio S/ϵ' . For 79 of the 80 samples, the ratio S/ϵ' was found to be smaller than 0.12, and for most the ratio was smaller than 0.05. The one exception was rock sample PW-30 (rock samples are identified by an identification number as shown in Table 3) for which ϵ' varied from 6.6 to 13.2. The reason for the variability was visible on the rock's surface; Fig. 4(a) shows a sketch of the surface of sample PW-30, which is a two-tone material comprised of a light-tone background and darker-tone inclusions. The sketch in Fig. 4(b) shows the permittivities measured at six locations on the surface of the sample; for locations not including the inclusion material, the measured value was 6.6, whereas for those partially or totally covering the inclusion material, the values were higher. Because of this large spatial variability in ϵ' , the sample was cut and only the "homogeneous" background portion was used in the analysis.

Figure 5 shows typical permittivity spectra for four rock samples, which exhibit no discernible dependence on frequency. This is characteristic of all samples measured in this study and is in agreement with previous conclusions reached by Olhoeff et al. [2]. Hence, in all forthcoming discussions and analyses, ϵ' will be treated as frequency independent and will be represented by the average value measured over

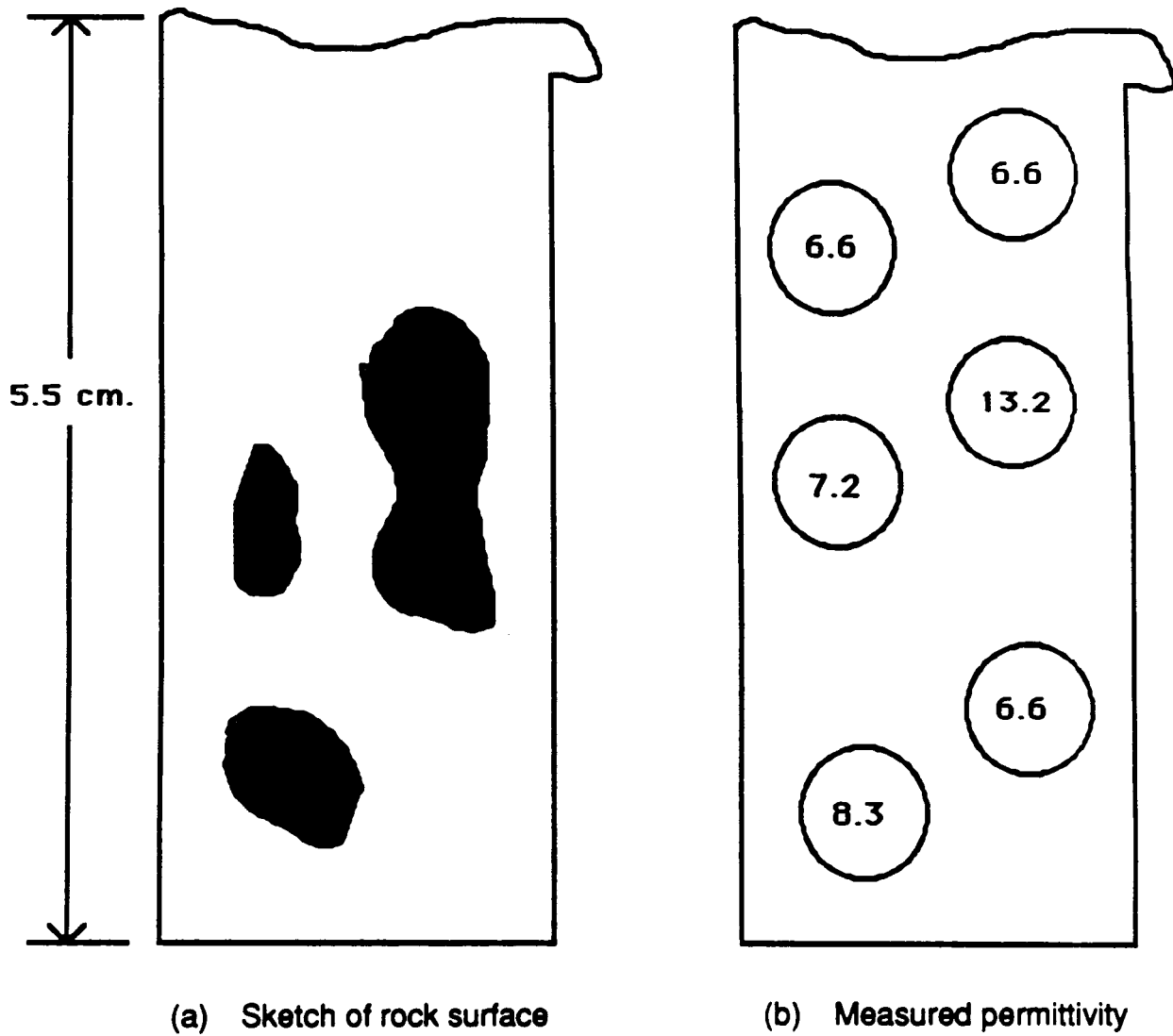


Fig. 4. This figure illustrates the spatial variability of the permittivity of sample G-PW-30. The dark areas in (a) consist of high iron content inclusions, and the circles in (b) show the locations at which the probe measurements were made.

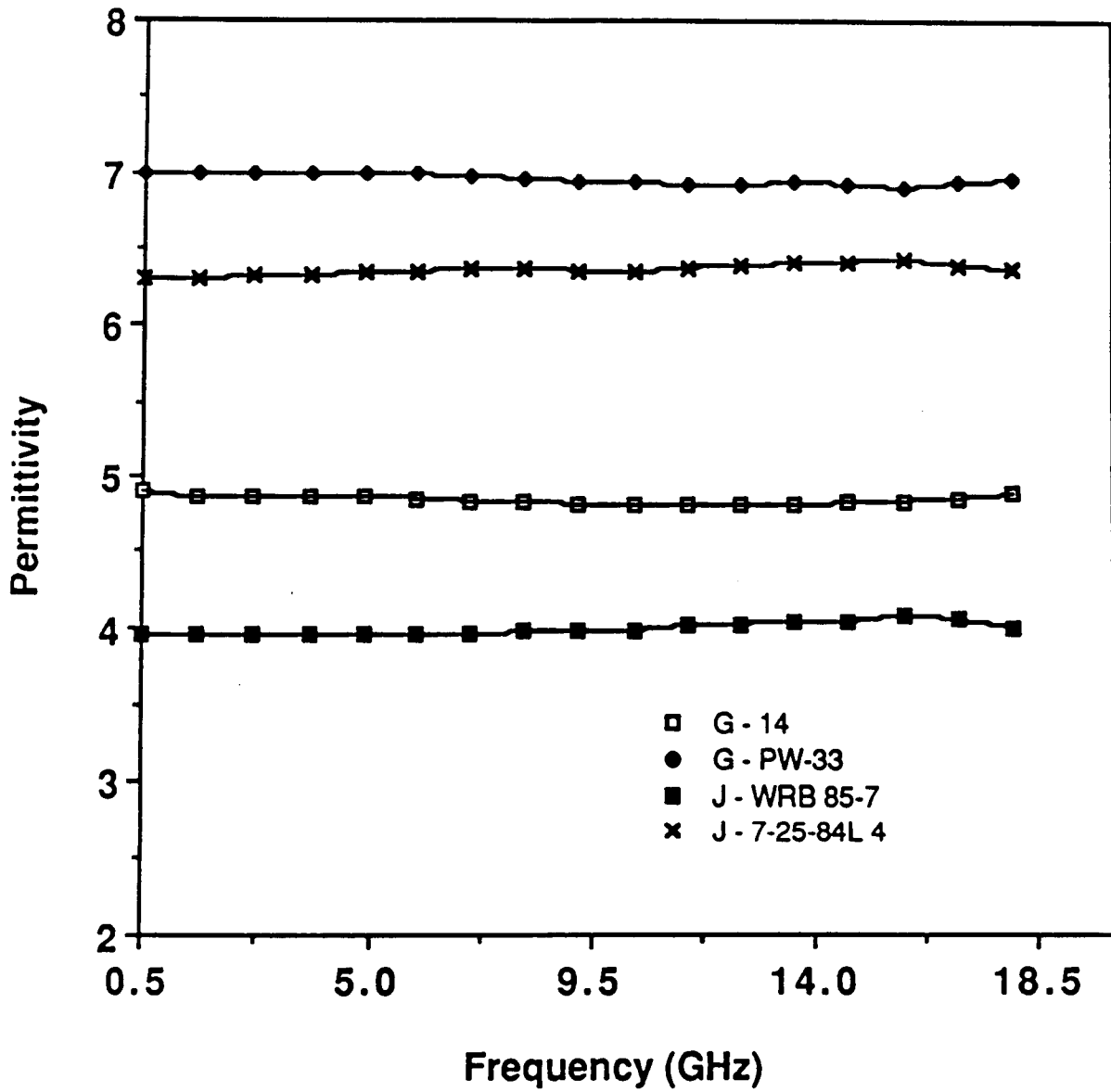


Fig. 5. Typical examples of measured permittivity spectra.

the 0.5-18 GHz range.

3. RESONANT-CAVITY PERTURBATION TECHNIQUE

A resonant cavity is a closed volume. Metal couplers protruding slightly into the cavity volume are used to measure the resonance characteristics of the cavity. The diagrams in Fig. 6 show a cylindrical cavity with two magnetic loop couplers protruding slightly into the cavity volume on the inside walls and connected to SMA connectors on the outside walls at a height midway between the top side (the lid) and the cavity floor. Figure 7 shows the measurement system.

With the cavity empty, if one were to connect a signal generator (HP 8350B in Fig. 7) to one of the connectors and a network analyzer to the other and then sweep the generator frequency across the resonance region of the cavity, the output power would be a Gaussian-like function of frequency (Fig. 8). This power spectrum is characterized by f_0 , the frequency at which the power is a maximum, and by Q_0 , the quality factor,

$$Q_0 = \frac{f_0}{\Delta f}, \quad (23)$$

where Δf is the half-power width of the power spectrum. If we insert a dielectric material into the cavity, the spectrum will change in two ways: 1) the resonant frequency decreases to a lower value, which we shall call f_S , and 2) the quality factor decreases to a lower value Q_S .

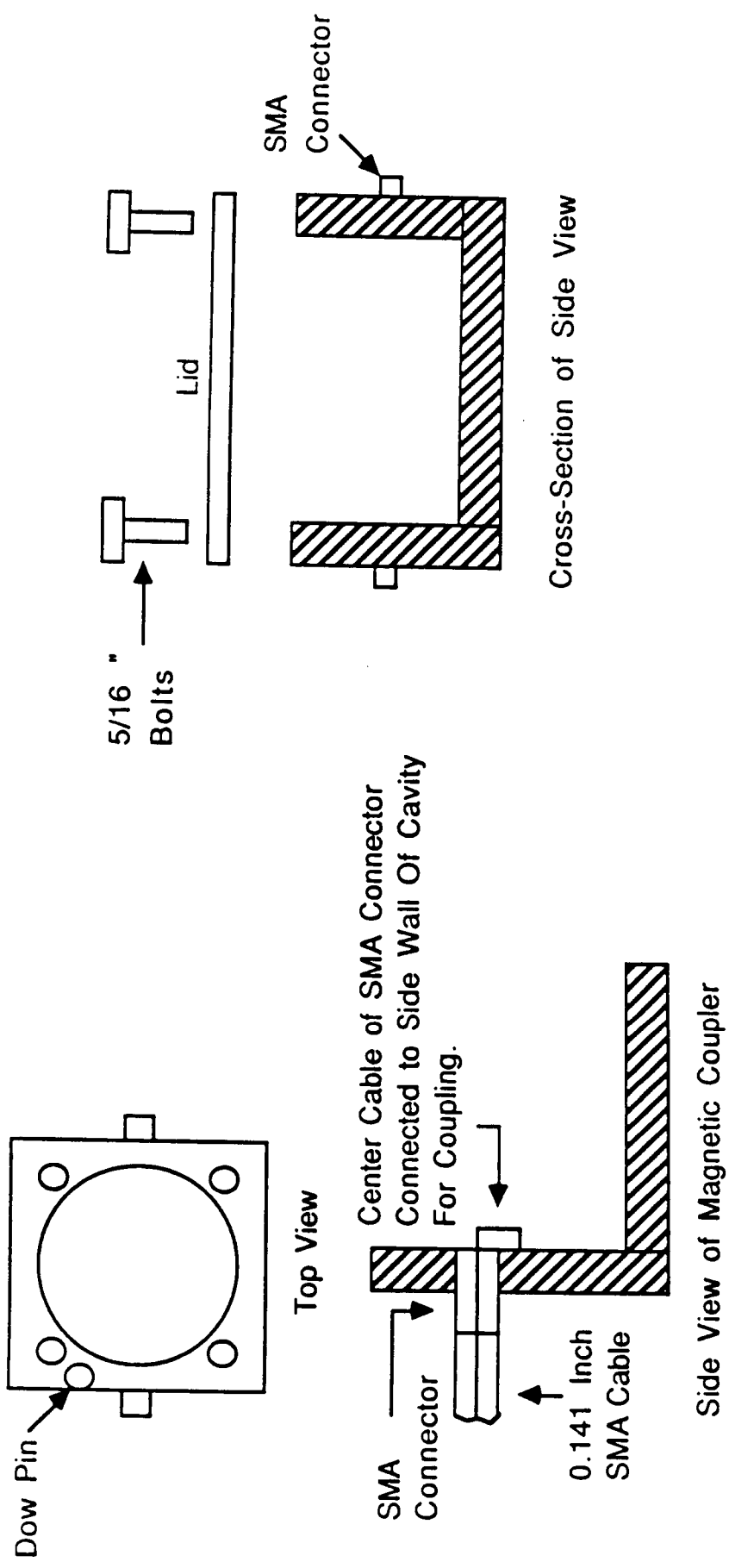


Fig. 6. Diagrams showing the coupling arrangements used with the cylindrical cavity.

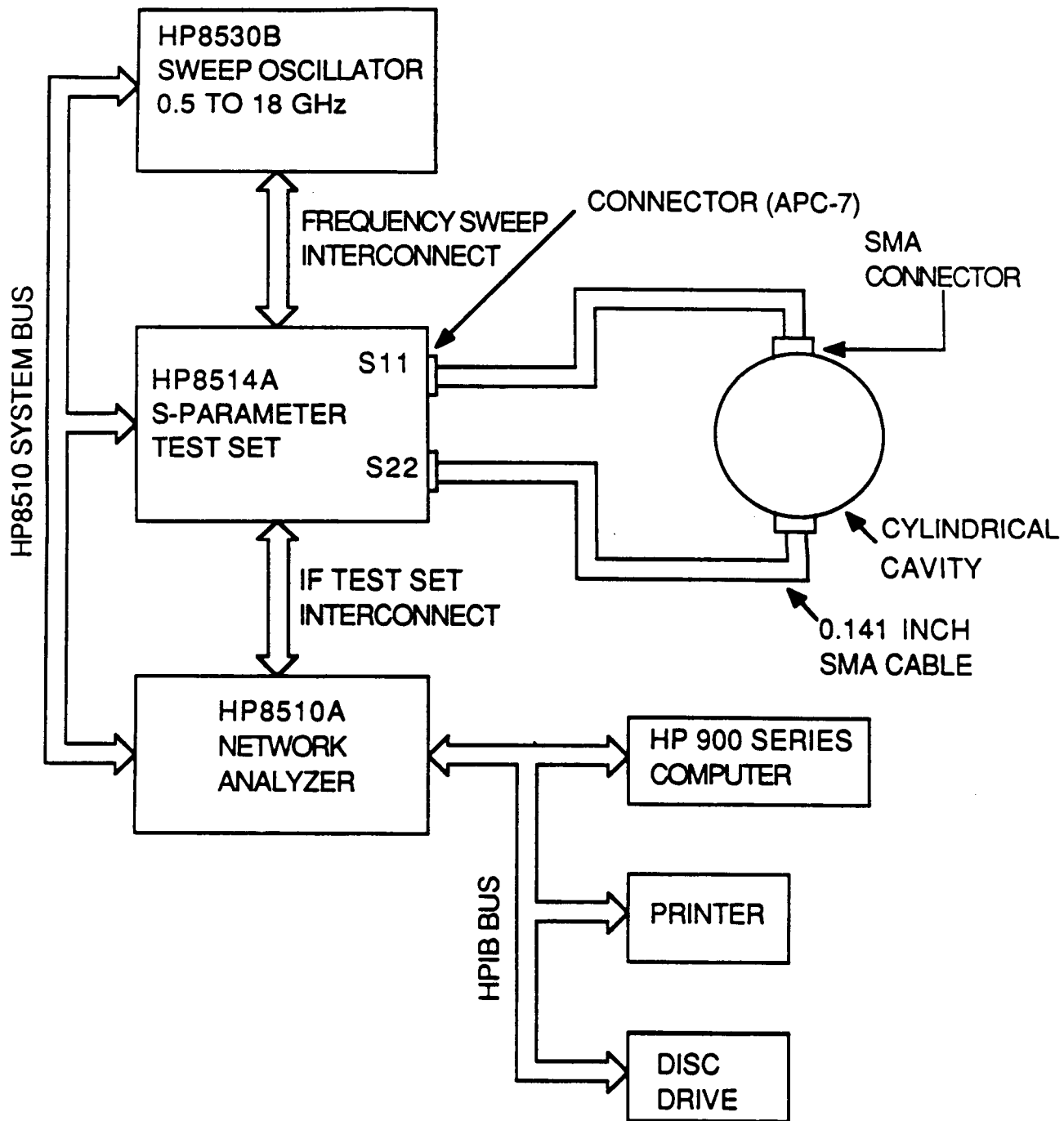


Fig. 7. Block diagram of the system used to measure the cavity transmission spectrum.

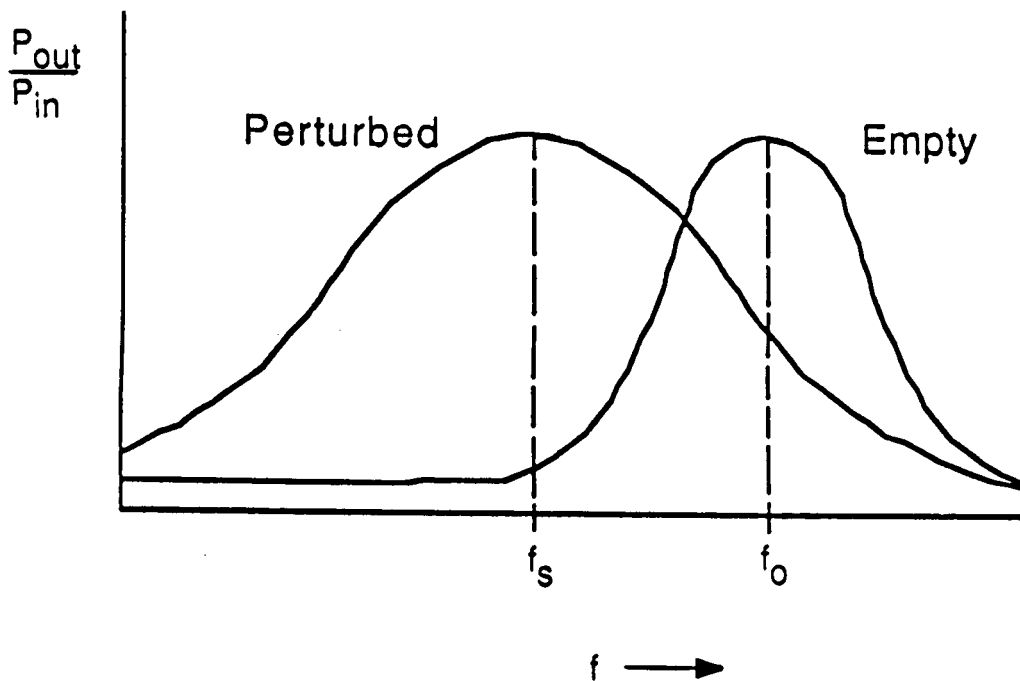
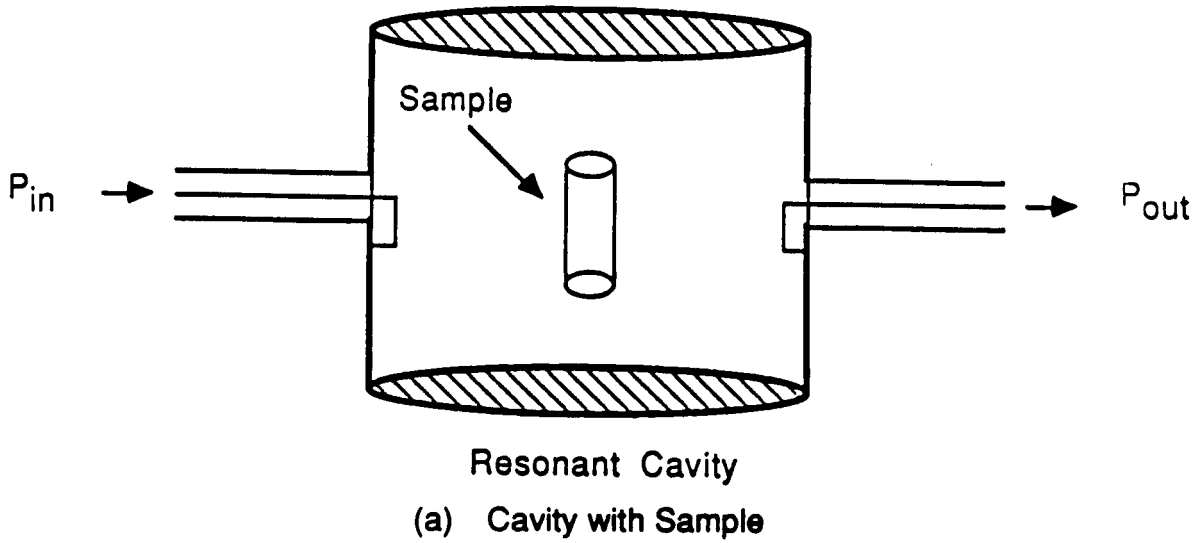


Fig. 8. When a sample is inserted in the cavity, its transmission spectrum changes: the resonant frequency shifts from f_0 to f_s and the spectrum becomes broader.

In order to maintain Q_s large (i.e., maintain a resonant-like spectrum), the volume of the material inserted into the cavity must be kept small relative to the cavity volume. When this is the case, the resonant-cavity perturbation technique [14] may be used to determine ϵ' and ϵ'' of a dielectric material from measurement of f_0 , f_s , Q_0 , and Q_s .

For a cylindrical cavity with radius a and height $d < 2a$ oscillating in the TM_{010} mode and containing a needle-shaped dielectric material oriented along the vertical axis of the cylinder, the shift in the resonant frequency is

$$\frac{f_s - f_0}{f_s} = -1.855 V(\epsilon' - 1) \quad (24)$$

if the volume fraction V is small. If the material has a dielectric loss factor ϵ'' , it can be shown [14, p. 373] that

$$\epsilon'' \cong \frac{(\epsilon' - 1)}{2} \left(\frac{f_0}{f_0 - f_s} \right) \left(\frac{1}{Q_s} - \frac{1}{Q_0} \right). \quad (25)$$

Solving (24) for ϵ' we get

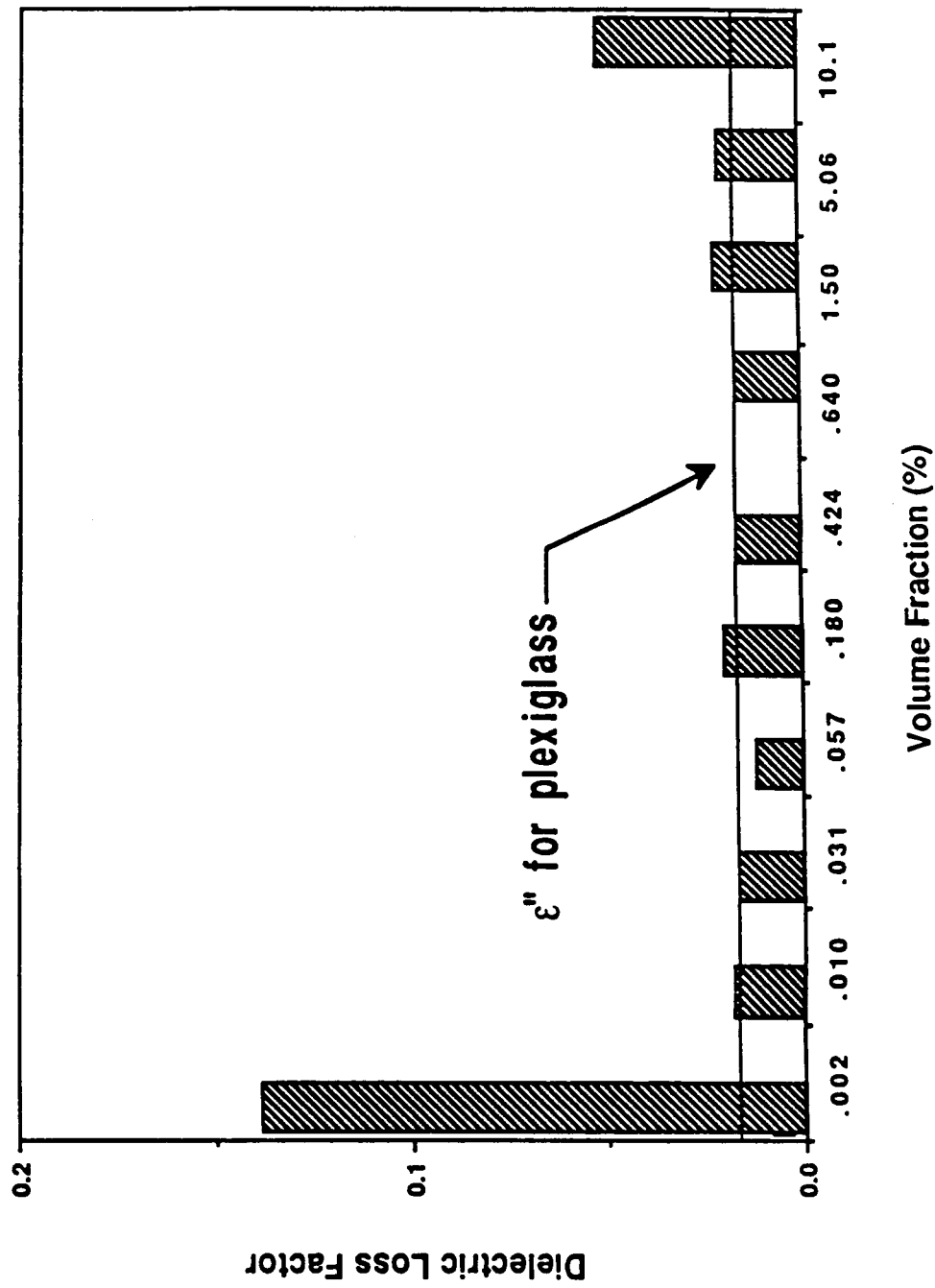
$$\epsilon' = 1 + \frac{f_0 - f_s}{1.855 f_s V}. \quad (26)$$

These expressions are valid only if V is very small, and (24) is valid only if the

dielectric material is approximately needle shaped and oriented vertically. One of the major problems associated with using this method to determine ϵ' and ϵ'' is the need to know V very accurately (ϵ'' depends on $(\epsilon' - 1)$ which, in turn, depends directly on $1/V$). In our case, however, we did not need to know V exactly because we already know ϵ' from the probe measurements discussed in the previous section. Hence, ϵ'' could be determined from (25) without the need to measure V . This procedure of using dielectric probes to measure ϵ' and resonant cavities to measure ϵ'' proved extremely effective because the errors associated with the handling and the measuring of the weight and volume of very small rock samples were intolerably high. As will be discussed below, a desirable value for V is about 0.5 percent. For a cavity volume of 2.5 cm^3 (which was the volume of one of the cavities used in this study), V would have to be about $1.25 \times 10^{-2} \text{ cm}^3$ and the corresponding weight would be about 31 mg (for a typical density of 2.5 g/cm^3).

3.1 Measurement Accuracy and Precision

By way of evaluating the measurement technique as well as establishing the range of validity of (25) as a function of V , we conducted a carefully designed experiment in which ϵ'' of plexiglass was measured as a function of V for values of V extending from 10^{-3} percent to 10.1 percent. We chose plexiglass because its complex dielectric constant is well known ($\epsilon = 2.55 - j 0.0165$) and its dielectric loss factor is small. The results of the experiment are shown in Fig. 9. The measurement



technique predicated the correct value for ϵ'' within a rms error of 0.001 for the range $0.01 \text{ percent} \leq V \leq 1 \text{ percent}$, and with a slightly larger error up to 5 percent. A detailed analysis of the errors associated with the measurements of the quantities f_0 , f_S , Q_0 , and Q_S led to the conclusion that the optimum range of V is between 0.5 percent and 1 percent, and that if V is in this range the minimum measurable value of ϵ'' is around 0.002.

The data tabulated in Table 3 are each an average of measurements conducted for five small samples of the parent sample.

3.2 Cavity Characteristics

Five cylindrical cavities were used in this study, with center frequencies ranging from 1.6 GHz to 16 GHz. Table 2 provides a listing of their pertinent characteristics. Of particular note is the cavity volume, ranging from approximately 1000 cm^3 for the 1.6 GHz cavity to only 1 cm^3 for the 16 GHz cavity.

3.3 Effects of Surficial Water

The data provided in Section 4 are based on measurements conducted after drying each rock sample in an oven at 100°C for 24 hours. The samples were dried to avoid the effects of surficial water on ϵ'' . For most of the samples, no discernible difference in ϵ'' was observed between measurements made before and after drying the sample (Fig. 10(a)), while for some the difference was quite significant (Fig. 10(b)).

Table 2. Characteristics of resonant cavities.

Cavity Frequency (GHz)	1.6	5	7.8	11.4	16
Resonant Frequency (GHz)	1.64	4.98	7.87	11.44	15.93
Q ₀ (empty cavity)	3000	1150	480	270	55
Height (cm)	6.34	2.06	1.25	0.82	0.65
Diameter (cm)	13.93	4.57	2.91	1.97	1.43
Volume of cavity (cm ³)	966.5	33.75	8.3	2.5	1.05

Table 3. Measured densities and dielectric constants of rocks.

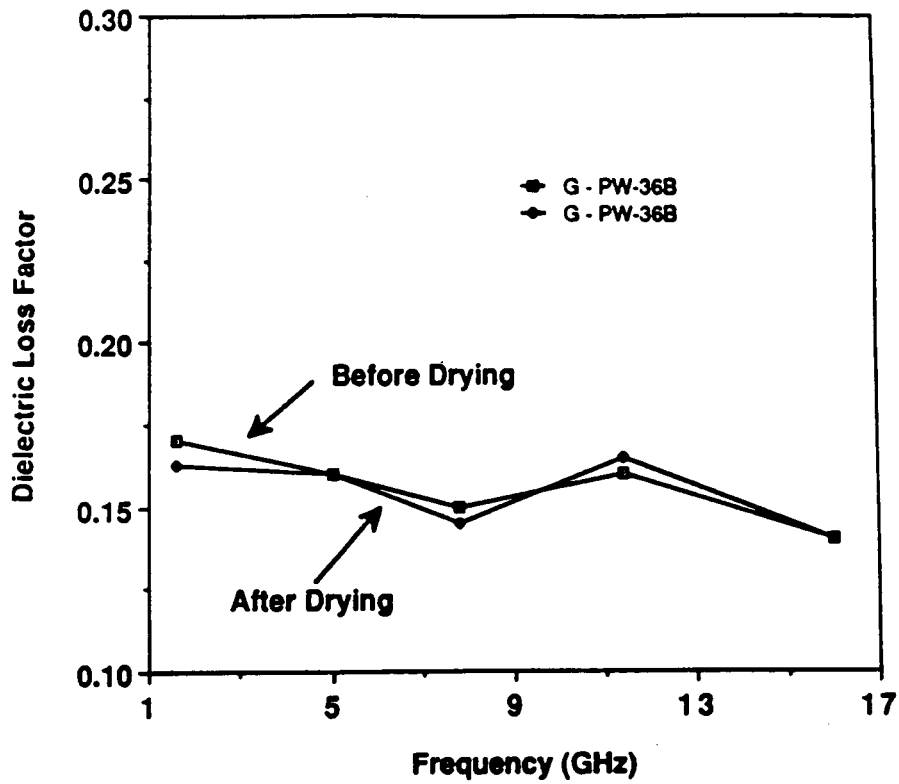
	A	B	C	D	E	F	G	H	I	J
1	A) Sulfates									
2	Rock Name	ID # *	Dens.**	E' ***	S/E' ****	E" (1.6)	E" (5.0)	E" (7.8)	E" (11.4)	E" (16.0)
3	gypsum	J - 7-27-84L 5A	1.89	3.90	0.070	< 0.002	< 0.002	< 0.002	< 0.002	< 0.002
4	B) Carbonates									
5	limestone	J - WRB 85-17	2.61	7.40	0.025	0.026	0.028	0.017	0.022	0.018
6	calcite	J - WRB 85-20	2.72	7.70	0.032	0.022	0.022	0.014	0.013	0.010
7	limestone	J - 7-21-84L 4	2.62	7.90	0.037	0.032	0.024	0.012	0.008	0.005
8	limestone	J - 7-23-84L 7	2.64	6.80	0.019	0.027	0.026	0.016	0.010	0.008
9	limestone	J - 7-25-84L 4	2.59	6.40	0.052	0.028	0.025	0.016	0.016	0.013
10	limestone	J - 7-25-84L 8	2.51	7.60	0.023	0.030	0.035	0.027	0.021	0.015
11	dolomite	J - 7-27-84L 2	2.60	6.80	0.026	0.036	0.032	0.027	0.018	0.015
12	dolomite	J - 7-27-84L 6A	2.62	6.50	0.030	0.027	0.014	0.010	0.005	0.008
13	dolomite	J - 7-27-84L 6G	2.64	6.70	0.026	0.031	0.012	0.009	0.005	0.007
14	calcareous sandst.	J - 7-27-84L 7J	2.60	7.00	0.062	0.074	0.048	0.047	0.040	0.036
15	C) Silicates									
16	1) Igneous									
17	a) Volcanic									
18	silicified volcanic	G - 3	2.58	4.80	0.022	0.014	0.016	0.010	0.010	
19	dacite/dellenite	G - 2	2.59	5.80	0.057	0.211	0.188	0.170	0.160	0.150
20	dacite - lava flow	G - 10	2.51	5.60	0.077	0.130	0.136	0.133	0.076	0.074
21	dacite - lava flow	G - 15	2.61	6.30	0.025	0.099	0.088	0.097	0.109	0.064
22	dacite/rhyodacite	G - 18	2.57	5.80	0.038	0.147	0.111	0.115	0.103	0.114
23	rhyolite - flow	G - 6	2.60	5.20	0.040	0.074	0.049	0.034	0.018	0.012
24	rhyolite clasts	G - 7-1	2.53	5.00	0.034	0.046	0.023	0.027	0.030	0.028
25	rhyolite - lava	G - 8-1	2.48	5.40	0.036	0.075	0.075	0.073	0.063	0.062
26	rhyolite - lava	G - 8'	2.46	5.20	0.050	0.080	0.075	0.045	0.026	0.020
27	rhyolite - tuff	G - 9	2.36	4.80	0.060	0.121	0.061	0.059	0.033	0.035
28	rhyolite - tuff	G - 12	2.07	4.00	0.067	0.035	0.021	0.023	0.026	
29	rhyolite - tuff	G - 13	1.88	3.70	0.042	0.050	0.042	0.037	0.033	0.035
30	rhyolite - tuff	G - 14	1.89	4.80	0.060	0.105	0.110	0.150	0.050	0.030
31	rhyolite - tuff	G - 17	2.41	6.00	0.056	0.158	0.147	0.154	0.154	0.168
32	andesite	G - PW-32	2.73	6.50	0.010	0.039	0.016	0.011	0.024	0.016

Table 3 (Cont.)

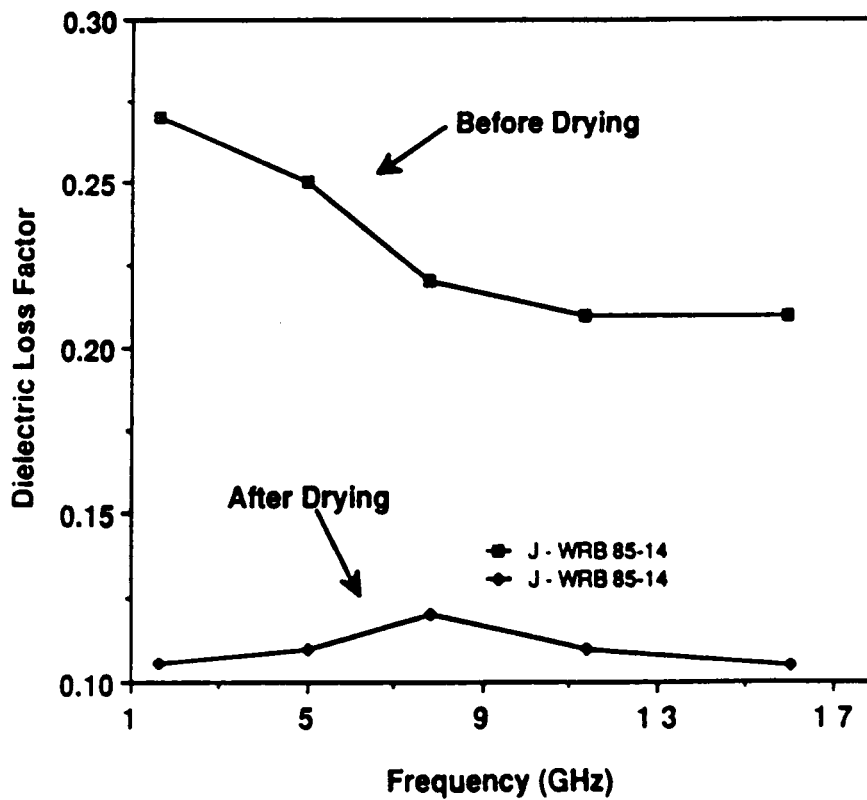
	A	B	C	D	E	F	G	H	I	J
	Rock Name	ID #	Dens. **	E' ***	S/E' ****	E* (1.6)	E* (5.0)	E* (7.8)	E* (11.4)	E* (16.0)
36	diabase	G - PW-33	3.03	6.60	0.040	0.112	0.083	0.057	0.075	0.062
37	basalt	G - PW-36A	2.93	7.30	0.025	0.180	0.184	0.180	0.165	0.170
38	basalt	G - PW-36B	2.90	7.60	0.024	0.158	0.161	0.160	0.159	0.167
39	diabase	G - PW-127	3.06	7.20	0.067	0.132	0.124	0.108	0.122	0.068
40	basalt	E - SP FLOW	2.31	6.10	0.060					
41	basalt	E - SP FLOW #1	2.35	6.00	0.032					
42	basalt	E - SP FLOW #8	2.11	5.50	0.079					
43	basalt	E - #2 SP MT	2.46	6.00	0.073					
44	basalt	E - #3 SP MT	1.43	3.60	0.093					
45	basalt	E - #4 SP MT	2.60	6.70	0.028					
46	oceanic basalt	G - Oc. Basalt	2.85	6.50	0.033	0.080	0.052	0.034	0.010	0.010
47	basalt/andesite	G - 1	2.92	7.60	0.024	0.111	0.108	0.097	0.094	0.094
48										
49										
50										
51										
52										
53	quartzite	G - PW-76	2.63	4.90	0.022	< 0.002	< 0.002	< 0.002	< 0.002	< 0.002
54	alk granite	G - PW-4	2.64	6.50	0.048	0.120	0.087	0.064	0.054	0.030
55	altered granodiorite	G - 4-2	2.56	5.30	0.056	0.048	0.054	0.028	0.035	0.020
56	tonalite	G - PW-24	2.69	5.90	0.081	0.048	0.031	0.023	0.025	0.021
57	diorite/quartz	G - 5	2.78	6.10	0.086	0.105	0.088	0.082	0.080	0.060
58	monzonite	G - PW-22	2.69	6.20	0.055	0.105	0.077	0.077	0.063	0.056
59	granodiorite	G - PW - 7	2.69	6.00	0.051	0.047	0.028	0.025	0.015	0.018
60	diorite	G - PW-25	2.89	6.50	0.052	0.052	0.027	0.022	0.028	0.027
61	gabbro (1)	G - PW-28	2.97	7.30	0.039	0.161	0.127	0.100	0.085	0.088
62	ol-gabbro (1)	G - PW-30	3.30	6.60	0.059	0.075	0.107	0.100	0.045	0.057
63	nephelinesyenite	G - PW-17	2.59	6.00	0.034	0.016	0.010	0.007	0.003	0.004
64	ijolite	G - PW-19	3.10	6.40	0.075	0.032	0.038	0.034	0.027	0.014
65	norite	G - PW-125	2.94	6.40	0.058	0.106	0.062	0.031	0.035	0.034
66	lamprophyre	G - PW-39	2.97	8.30	0.021	0.101	0.078	0.077	0.068	0.059
67	pyroxenite	G - PW-40	2.98	7.00	0.028	0.238	0.149	0.194	0.081	0.116
68	dunite	G - PW-41	3.16	6.10	0.030	0.021	0.024	0.022	0.023	0.023
69										

A		B		C		D		E		F		G		H		I		J	
71	Rock Name	ID #		Dens.	E'	S/E'	E*	E* (1.6)	E* (5.0)	E* (7.8)	E* (11.4)	E* (16.0)							
72																			
73	2) Sedimentary																		
74																			
75	sandstone (2)	J - WRB 85-1		2.13	2.50	0.118	0.015	0.014	0.013	0.006		0.005							
76	sandstone (2)	J - WRB 85-2		2.53	6.00	0.030	0.077	0.061	0.035	0.042		0.035							
77	sandstone (2)	J - WRB 85-3		2.29	4.00	0.075	0.028	0.031	0.015	0.017		0.014							
78	sandstone (2)	J - WRB 85-4		2.12	3.40	0.084	0.035	0.041	0.024	0.019		0.014							
79	sandstone (2)	J - WRB 85-5		2.10	3.70	0.060	0.042	0.044	0.027	0.012		0.017							
80	sandstone (2)	J - WRB 85-6		2.23	5.30	0.055	0.112	0.126	0.081	0.090		0.074							
81	sandstone (2)	J - WRB 85-7		2.33	4.00	0.093	0.040	0.033	0.028	0.013		0.010							
82	sandstone (2)	J - WRB 85-8		2.19	3.50	0.037	0.021	0.020	0.020	0.015		0.014							
83	bentonite	J - WRB 85-11		2.35	5.70	0.049	0.220	0.200	0.201	0.200		0.185							
84	shale (3)	J - WRB 85-12		2.23	4.80	0.025	0.082	0.065	0.031	0.045		0.035							
85	sandstone	J - WRB 85-13		2.41	4.30	0.120	0.076	0.050	0.038	0.032		0.028							
86	siltstone (4)	J - WRB 85-14		2.57	5.60	0.032	0.120	0.110	0.110	0.111		0.105							
87	sandstone (5)	J - WRB 85-15		2.38	3.10	0.080	0.024	0.022	0.015	0.011		0.010							
88	shale	J - WRB 85-18		2.33	5.40	0.049	0.140	0.120	0.062	0.039		0.024							
89	shale	J - WRB 85-19		2.33	5.30	0.074	0.140	0.167	0.078	0.040		0.030							
90	siltstone	J - 7-21-84L 6		2.15	4.80	0.033	0.080	0.080	0.075	0.070		0.070							
91	sandstone	J - 7-23-84L 4		2.26	3.00	0.047	0.030	0.020	0.015	0.014		0.013							
92	sandstone	J - 7-23-84L 11		2.48	5.00	0.026	0.040	0.021	0.018	0.010		0.010							
93	siltstone	J - 7-23-84L 14		2.37	6.50	0.019	0.038	0.028	0.014	0.011		0.012							
94	sandstone	J - 7-25-84L 6		2.45	4.70	0.036	0.050	0.036	0.031	0.014		0.013							
95	siltstone	J - 7-27-84L 8I		2.36	5.90	0.015	0.245	0.240	0.235	0.150		0.140							
96	sandstone	E - TB-19		2.08	2.90	0.058													
97	Other																		
98	N/A	G - 5'		2.68	6.10	0.098	0.100	0.051	0.061	0.049		0.035							
99	Elgygytyn	G - Elgy (7)		2.36	5.60	0.030	0.030	0.034	0.028	0.027		0.024							
100	apirite	G - PW-101		2.63	5.40	0.031	< 0.002	< 0.002	< 0.002	< 0.002		< 0.002							
101	alkalic	G - PW-14		2.65	5.60	0.071	0.074	0.072	0.065	0.052		0.041							

- Identification Number
 - J - JPL (Jet Propulsion Laboratory)
 - G - GSFC (Goddard Space Flight Center)
 - E - ERIM (Environmental Research Institute of Michigan).
- ** Density of Rock Sample (g/cm³).
- *** Permittivity of measurements was averaged over the range of 0.5 to 18 GHz.
- **** (Standard deviation of the permittivity measurements)/
 - (1) Sample contained large inclusions and is removed from all analysis, data recorded in Table 4.1 is for the non-inclusion part of the rock.
 - (2) Frontier Formation.
 - (3) Mawry Formation.
 - (4) Thermopolis Formation.
 - (5) Cloverlea Formation.
 - (6) Sundance Formation.



(a) Sample PW-36B



(b) Sample WRB-85-14

Fig. 10. Whereas oven-drying sample PW-36B had no influence on its ϵ'' , it had a large effect on sample WRB 85-14.

For a few of the measured samples, ϵ'' was observed to exhibit no discernible dependence on frequency. For most samples, however, ϵ'' decreased with increasing frequency over the 1.6 GHz - 16 GHz range. Typical examples of these two types of spectra are shown in Fig. 11.

4. MEASURED DATA

The measured dielectric data is given in Table 3. The entries include 1) rock type, 2) rock #, which designates the source (G = NASA/GSFC, J = NASA/JPL, and E = ERIM) and associated numbers, 3) density, 4) ϵ' (average value over the 0.5 - 18 GHz range), 5) S/ϵ' , the standard derivation-to-mean ratio of the measured value of ϵ' , and 6-10) are entries for ϵ'' at 1.6, 5.0, 7.8, 11.4, and 16.0 GHz.

Table 4 lists the bulk chemical properties of the rock samples from x-ray fluorescence. The properties of samples with a G designation were measured by or for NASA/GSFC, and the properties of those with a J designation were measured by the Geology Department at the University of Michigan. To date 56 of the 80 rock samples have been analyzed for mineral composition.

5. ANALYSIS OF PERMITTIVITY DATA

5.1 Distribution of Measured Data

Among the 80 rock samples, the measured value of ϵ' ranged between 2.5 and 8.3. These values are presented in horizontal bar-chart format in Fig. 12, and a similar

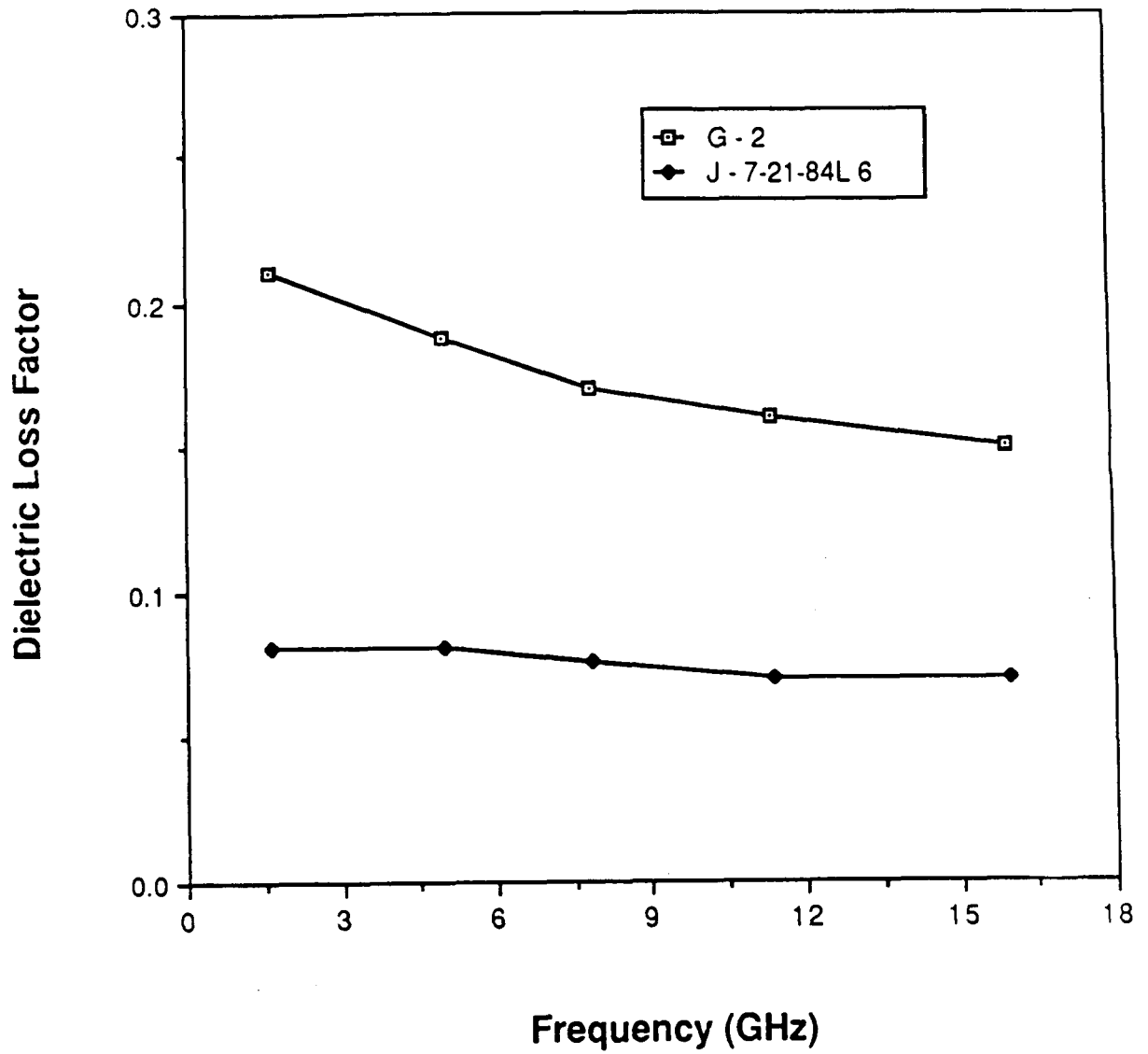


Fig. 11. Typical examples of the measured spectra of the dielectric loss factor ϵ'' .

Table 4. Mineral composition of the rock samples.

	A	B	C	D	E	F	G	H	I	J	K	L	M	N	O
1	A) Sulfates														
2															
3	ID # *	Dens.**	Fe2O3	FeO	Fe2O3T@	TiO2	CaO	K2O	SiO2	Al2O3	MgO	Na2O	P2O5	MnO	LOI***
4	J - 7-27-84L 5A	1.89													
5	B) Carbonates														
6															
7	J - WRB 85-17	2.61													
8	J - WRB 85-20	2.72													
9	J - 7-21-84L 4	2.62													
10	J - 7-23-84L 7	2.64													
11	J - 7-25-84L 4	2.59													
12	J - 7-25-84L 8	2.51													
13	J - 7-27-84L 2	2.60													
14	J - 7-27-84L 6A	2.62													
15	J - 7-27-84L 6G	2.64													
16	J - 7-27-84L 7J	2.60													
17	C) Silicates														
18	1) Igneous														
19	a) Volcanic														
20															
21	G - 3	2.58			0.10	0.67	0.20	0.00	96.30	1.00	0.50	1.20	0.00	0.05	
22	G - 2	2.59			4.50	0.70	3.60	3.10	65.00	15.40	2.38	3.52	0.19	0.09	
23	G - 10	2.51			6.20	1.05	4.90	2.40	61.50	17.50	1.20	3.85	0.33	0.05	
24	G - 15	2.61			6.10	0.77	5.20	2.90	61.70	17.10	2.50	3.40	0.16	0.06	
25	G - 18	2.57			4.50	0.78	3.30	3.30	66.70	16.30	0.80	3.80	0.31	0.05	
26	G - 6	2.60			1.60	0.10	0.30	3.60	74.90	15.60	3.90	0.00	0.04	N/A	
27	G - 7-1	2.53			0.00	0.59	0.20	0.20	82.00	15.50	0.10	1.30	0.21	0.04	
28	G - 8-1	2.48			1.90	0.30	1.40	4.90	73.20	15.30	0.40	3.10	0.05	0.00	
29	G - 8'	2.46			1.60	0.31	0.80	5.20	72.80	15.70	0.40	3.10	0.05	0.04	
30	G - 9	2.36			1.70	0.26	1.40	4.70	73.40	14.80	0.80	3.00	0.08	0.06	
31	G - 12	2.07			1.10	0.14	1.90	4.80	75.50	13.00	0.10	3.40	0.12	0.08	
32	G - 13	1.88			1.30	0.16	0.90	6.10	75.30	13.50	0.30	2.30	0.04	0.06	
33	G - 14	1.89			1.40	0.17	2.50	4.50	76.30	13.50	0.90	0.70	0.00	0.06	
34	G - 17	2.41			1.70	0.23	0.60	4.60	75.00	14.50	0.25	2.85	0.08	0.09	
35	G - PW-32	2.73	1.15	1.08	2.35	0.73	9.65	1.16	53.41	25.79	0.25	5.31	0.04	0.02	2.25

Table 4 (Cont.)

A	B	C	D	E	F	G	H	I	J	K	L	M	N	O
ID #	Dens.	Fe2O3	FeO	Fe2O3T	TiO2	CaO	K2O	SiO2	Al2O3	MgO	Na2O	P2O5	MnO	LOI
36														
37	G - PW-33	1.16	8.44	10.56	0.86	11.74	0.45	52.51	12.82	9.81	1.61	0.09	0.17	0.98
38	G - PW-36A	2.59	7.94	11.43	1.07	11.26	0.40	51.02	14.02	7.86	1.77	0.12	0.17	2.55
39	G - PW-36B	2.59	7.94	11.43	1.07	11.26	0.40	51.02	14.02	7.86	1.77	0.12	0.17	2.55
40	G - PW-127	1.35	8.34	10.64	0.94	11.70	0.47	52.41	13.11	9.36	1.64	0.07	0.17	0.80
41	E - SP FLOW													
42	E - SP FLOW #1													
43	E - SP FLOW #8													
44	E - #2 SP MT													
45	E - #3 SP MT													
46	E - #4 SP MT													
47	E - Oc. Basalt													
48	G - 1			8.50	1.28	8.20	0.80	49.90	17.60	8.00	3.20	0.47	0.09	
49														
50	b) Plutonic													
51														
52														
53	G - PW-76	0.02	0.05	0.08	0.02	0.00	0.03	100.00	0.24	0.01	0.00	0.00	0.00	0.20
54	G - PW-4	2.11	1.60	3.89	0.21	0.39	4.94	73.44	12.29	0.02	4.96	0.00	0.08	0.56
55	G - 4-2			5.00	0.54	0.80	3.60	65.00	16.00	2.50	4.10	0.25	0.01	
56	G - PW-24	1.41	4.08	5.95	0.67	2.39	1.30	63.08	16.88	5.98	3.56	0.10	0.09	1.06
57	G - 5			6.60	1.05	5.90	1.80	57.90	16.70	5.80	4.30	0.44	0.12	
58	G - PW-22	3.60	2.84	6.76	0.77	4.13	4.17	61.42	15.95	2.32	3.48	0.25	0.11	1.37
59	G - PW-7	1.38	3.22	4.97	0.62	4.19	3.91	64.20	15.44	2.25	3.78	0.23	0.14	0.70
60	G - PW-25	2.38	5.34	8.33	1.27	9.48	1.18	49.81	19.35	6.16	3.86	0.08	0.08	1.41
61	G - PW-28 (1)	6.26	8.34	15.55	1.49	12.61	0.16	44.20	17.82	5.30	1.80	0.04	0.16	1.11
62	G - PW-30 (1)	2.42	12.43	16.26	5.21	6.88	1.33	45.28	16.32	4.33	3.67	0.76	0.17	1.34
63	G - PW-17	0.23	1.06	1.41	0.03	0.16	5.18	59.65	22.07	0.04	9.69	0.00	0.02	0.93
64	G - PW-19	2.60	7.32	10.75	2.60	12.13	3.93	43.08	13.10	9.66	3.49	0.54	0.20	1.87
65	G - PW-125	2.63	7.09	10.53	2.52	4.96	0.27	48.42	19.66	10.83	2.87	0.03	0.09	1.15
66	G - PW-39	4.21	7.34	12.38	1.57	12.06	1.49	45.94	16.09	6.53	3.04	0.62	0.19	1.47
67	G - PW-40	2.36	10.78	14.36	1.10	6.43	0.74	48.23	12.31	12.95	1.85	0.06	0.22	3.16
68	G - PW-41	1.62	7.47	9.94	0.00	0.05	0.00	39.57	0.44	47.60	0.00	0.00	0.16	2.85
69														
70														

Table 4 (Cont.)

A		B	C	D	E	F	G	H	I	J	K	L	M	N	O	
ID #		Dens.	Fe2O3	FeO	Fe2O3T	TiO2	CaO	K2O	SiO2	Al2O3	MgO	Na2O	P2O5	MnO	LOI	
71																
72																
73	2) Sedimentary															
74																
75	J - WRB 85-1	2.13			0.81	0.11	0.68	1.82	91.08	6.47	0.00	1.01	0.08	0.02	1.20	
76	J - WRB 85-2	2.53			29.72	0.10	0.83	1.44	58.79	6.17	0.28	0.71	0.26	2.63	6.79	
77	J - WRB 85-3	2.29			0.80	0.09	0.75	2.11	89.37	7.34	0.00	1.11	0.04	0.02	1.29	
78	J - WRB 85-4	2.12			1.18	0.24	1.01	1.67	90.29	6.42	0.06	1.09	0.27	0.02	1.41	
79	J - WRB 85-5	2.10			0.98	0.20	0.70	1.63	91.93	5.97	0.04	0.94	0.16	0.02	1.42	
80	J - WRB 85-6	2.23			34.40	0.19	0.89	1.45	55.39	5.98	0.32	0.50	0.27	2.16	7.68	
81	J - WRB 85-7	2.33			1.44	0.11	0.65	2.32	88.85	7.15	0.00	0.97	0.11	0.02	1.44	
82	J - WRB 85-8	2.19			0.73	0.08	0.70	1.86	88.86	6.87	0.00	1.02	0.08	0.01	1.24	
83	J - WRB 85-11	2.35			1.43	0.11	0.90	0.60	86.98	9.49	0.35	1.77	0.03	0.01	6.41	
84	J - WRB 85-12	2.23			0.90	0.29	0.37	2.67	90.17	7.57	0.23	0.08	0.07	0.01	3.55	
85	J - WRB 85-13	2.41			5.34	0.71	1.16	0.21	81.99	9.27	0.00	0.00	0.01	0.02	5.71	
86	J - WRB 85-14	2.57			7.57	0.70	0.35	1.25	79.35	11.62	0.82	0.38	0.28	0.09	5.78	
87	J - WRB 85-15	2.38			0.89	0.24	0.16	0.20	90.79	7.45	0.00	0.00	0.01	0.02	3.00	
88	J - WRB 85-18	2.33			1.40	0.13	0.81	0.62	88.04	9.17	0.26	1.96	0.03	0.01	5.88	
89	J - WRB 85-19	2.33			1.22	0.11	0.88	0.54	85.77	8.56	0.27	1.99	0.04	0.01	5.92	
90	J - 7-21-84L 6	2.15			1.23	0.35	0.40	2.69	88.21	8.75	0.35	0.11	0.08	0.01	7.19	
91	J - 7-23-84L 4	2.26			0.28	0.07	0.12	0.09	96.57	2.67	0.00	0.00	0.02	0.02	1.26	
92	J - 7-23-84L 11	2.48			2.51	0.11	10.76	1.63	82.49	5.36	0.15	0.38	0.10	0.07	8.82	
93	J - 7-23-84L 14	2.37														
94	J - 7-25-84L 6	2.45			0.51	0.41	13.65	1.61	78.65	5.73	0.96	1.49	0.09	0.06	10.14	
95	J - 7-27-84L 8I	2.36			1.25	0.10	0.91	0.62	88.50	8.85	0.26	1.85	0.03	0.02	5.90	
96	E - TB-19	2.08														
97	Other															
98	G - 5'	2.68														
99	G - Elgy (7)	2.36														
100	G - PW-101	2.63	0.04	0.30	0.34	0.03	1.39	3.55	75.80	13.99	0.14	4.31	0.00	0.01	0.38	
101	G - PW-14	2.65	2.54	1.63	4.36	0.68	3.08	5.72	55.28	19.93	0.84	7.46	0.19	0.07	2.11	

presentation is given in Fig. 13 for the rock groups identified in Tables 3 and 4.

5.2 Dependence on Density

According to previous studies [1-6], the density ρ (g/cm³) is the single most important parameter governing the magnitude of ϵ' . One of the commonly used formulas relating ϵ' to ρ is based on a simple model relating ϵ'_p of a powder material of density ρ_p to that of the parent (solid) rock material of permittivity ϵ and density ρ through

$$\begin{aligned} (\epsilon'_p)^{1/\rho_p} &= (\epsilon)^{1/\rho} (\epsilon_a)^{1/\rho_a} \\ &= (\epsilon)^{1/\rho} , \end{aligned} \tag{27}$$

where $\epsilon_a = 1$ and $\rho_a = 1$ are the permittivity and density of air. Campbell and Ulrichs [1] conducted measurements for a large number of powdered rocks, all at a density $\rho_p = 1 \text{ g/cm}^3$, and found that ϵ'_p varied over the narrow range between 1.9 and 2.1 for most of the 25 different types of powdered rocks measured and that the mean value is around 2.0. Upon setting $\rho_p = 1 \text{ g/cm}^3$ and $\epsilon'_p = 2$ in (27), we get

$$\epsilon' = 2^\rho . \tag{28}$$

This result is in close agreement with the formula used by Olhoeft and Strangway [4],

$$\epsilon' = (1.93 \pm 0.17)^\rho , \tag{29}$$

in their analysis of moon rocks. For the data measured in the present study, an

equation of the form $\epsilon' = A^\rho$ was used to fit the data and the value $A = 1.96$ was found

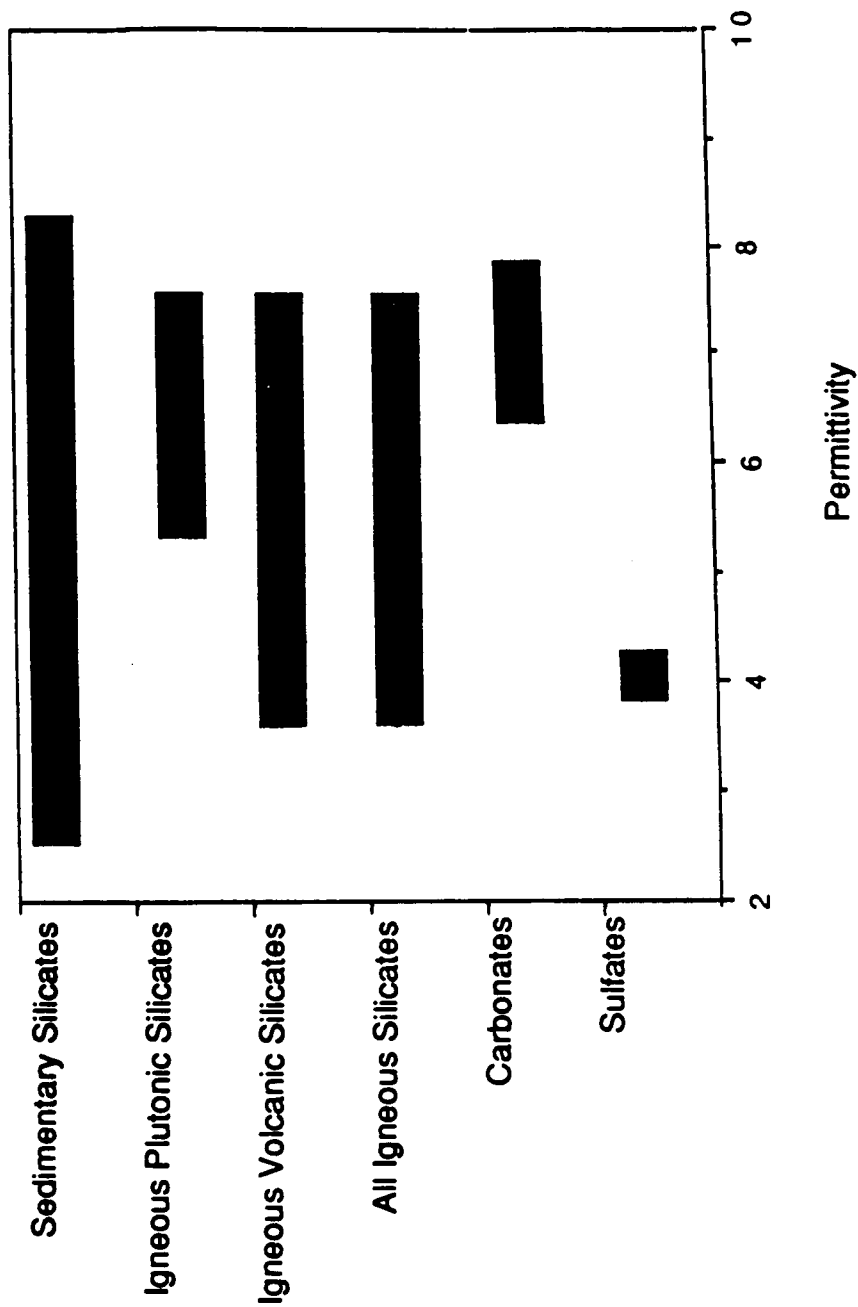


Fig. 13. Range of ϵ' for individual rock types.

to give the minimum mean-square-error. The function

$$\epsilon' = 1.96\rho^2, \quad (30)$$

is shown in Fig. 14, together with the measured data. The linear correlation coefficient between the values predicted by (30) and the measured values of ϵ' is $R = 0.72$. The data scatter about the regression curve is attributed to the dependence of ϵ' on the mineral composition of the rocks.

Also, the data was used to generate first-, second-, and third-order polynomial regressions relating $(\epsilon' - 1)$ to ρ . The results are:

$$\epsilon' - 1 = 1.86\rho, \quad (31a)$$

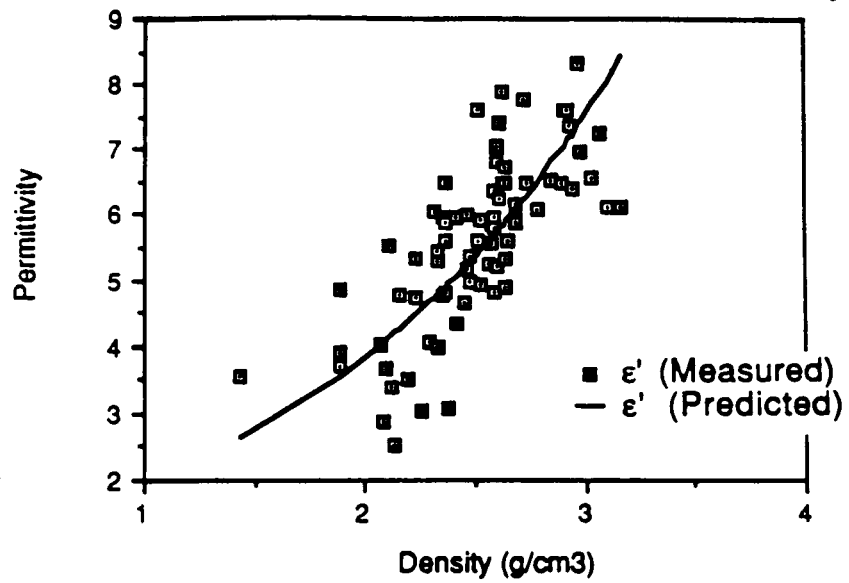
$$\epsilon' - 1 = 0.61\rho + 0.49\rho^2, \quad (31b)$$

$$\epsilon' - 1 = 1.0\rho - 0.11\rho^3, \quad (31c)$$

and in all cases the linear correlation coefficient between the measured value of ϵ' and the value predicted by any of the above equations was $R = 0.73$. Thus, statistically speaking, the model given by (30) offers a fit to the data comparable to that provided by the simple linear model given by (31a), which is shown in Fig. 15.

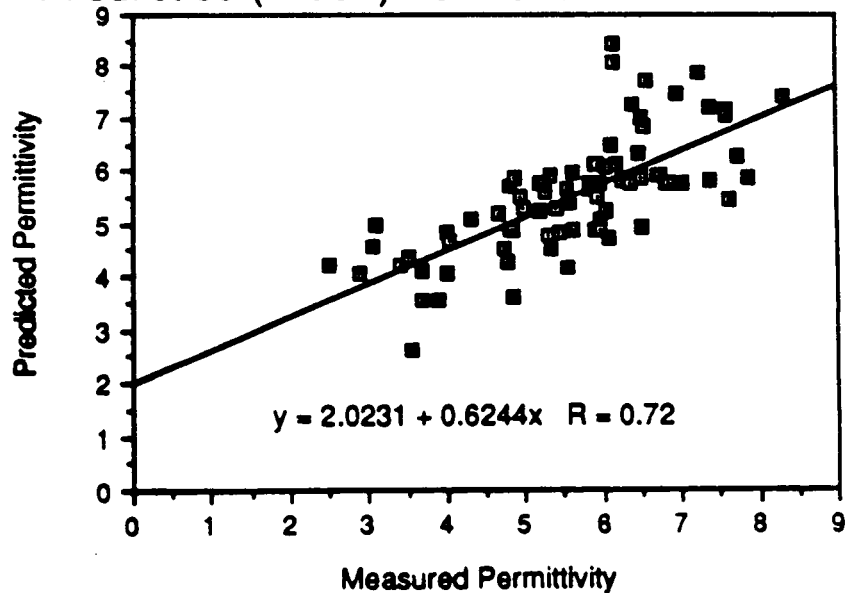
The variation of ϵ' with ρ is shown in Fig. 16 for individual rock types. The carbonates exhibit the narrowest density range, followed by the igneous plutonic silicates, and then by the igneous volcanic silicates and the sedimentary silicates. The igneous volcanic silicates have the strongest slope for ϵ' versus ρ .

Measured and Predicted (1.96^{ρ}) vs. Density



(a) ϵ' versus density

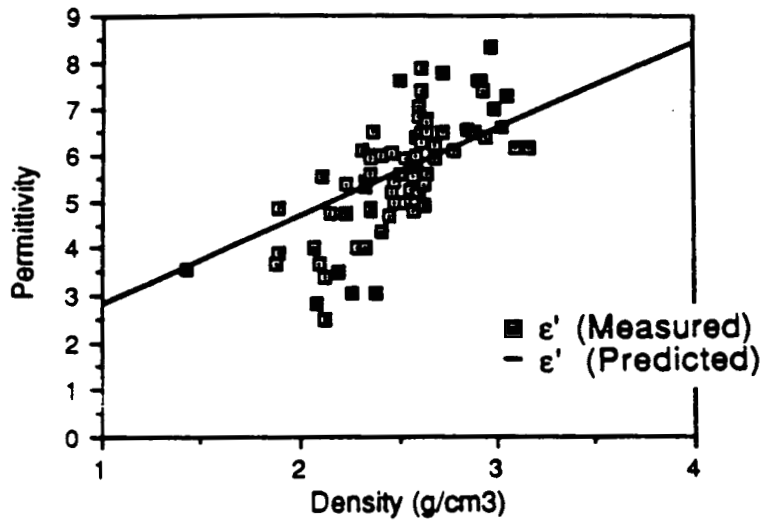
Predicted (1.96^{ρ}) vs. Measured Permittivity



(b) ϵ'_p versus ϵ'_m

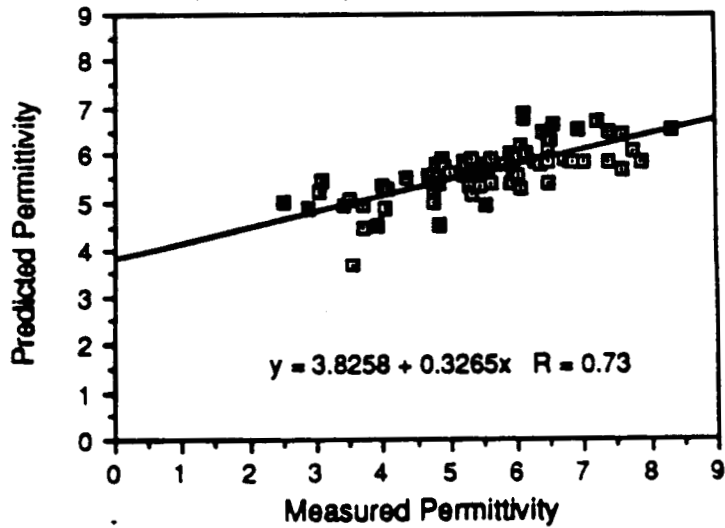
Fig. 14. Measured permittivity ϵ'_m and predicted permittivity $\epsilon'_p = 1.96^{\rho}$, both plotted against density in (a) and against each other in (b).

Measured and Predicted ($1 + 1.86\rho$) vs. Density



(a) ϵ' versus density

Predicted ($1 + 1.86\rho$) vs. Measured Permittivity



(b) ϵ'_p versus ϵ'_m

Fig. 15. Measured permittivity ϵ'_m and predicted permittivity $\epsilon'_p = 1 + 1.86\rho$, both plotted against density in (a) and against each other in (b).

Permittivity versus Density

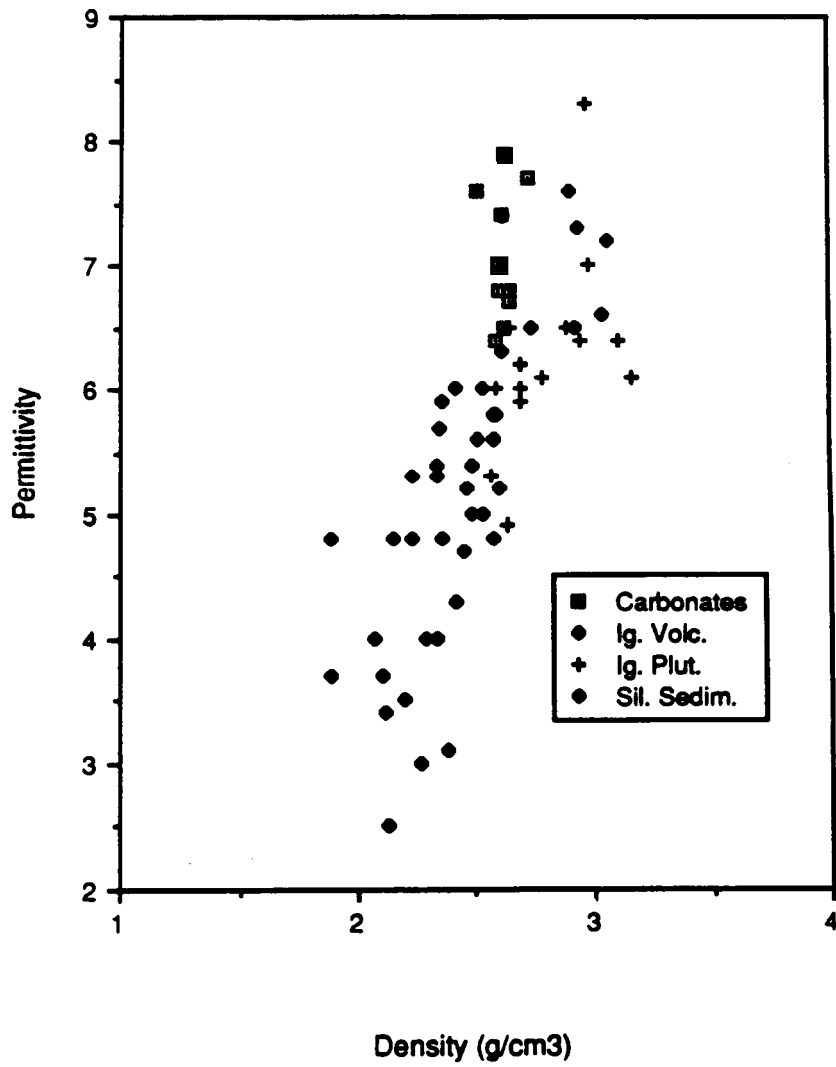


Fig. 16. Permittivity versus density for individual rock types.

5.3 Dependence on Mineral Composition

Stepwise multivariate regression analysis was performed (using BMDP) to evaluate the statistical correlation between the measured ϵ' of the rock samples and their bulk chemical composition. The analysis was performed for individual types of rocks as well as for combinations of rock types.

5.3.1 Igneous Volcanic Silicates

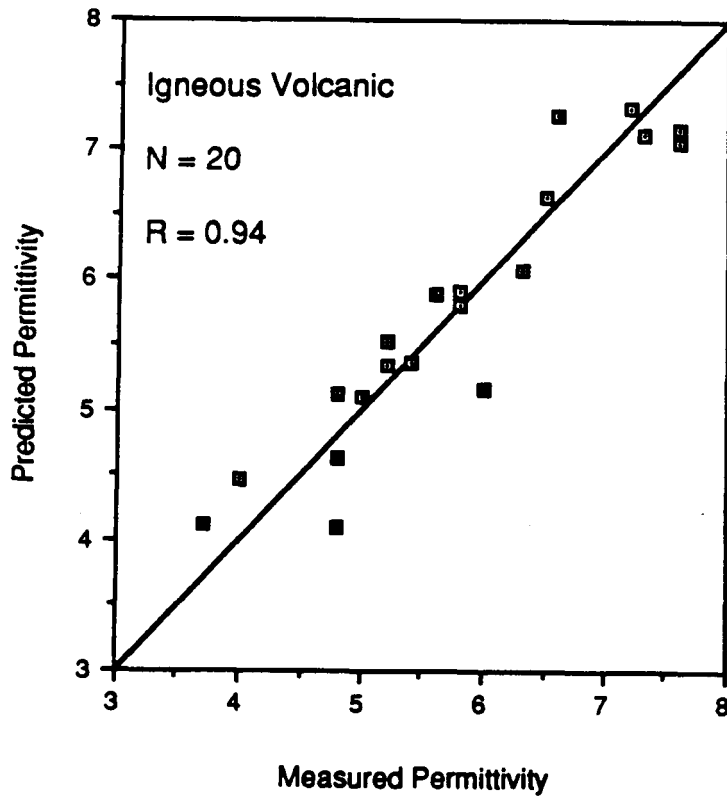
For the 20 silicate samples classified as igneous volcanic rocks, the stepwise regression analysis selected density as the most important variable. According to Table 5, density accounts for 76% of the total variance (see the R-squared entry in the table), the combination of density and SiO₂ content accounts for 88% of the variance, and the other elements are each responsible for small incremental improvements in the variance. With density and SiO₂ content, we obtain a linear correlation coefficient of 0.94 between the measured value of ϵ' and the value computed using the linear regression equation given in Fig. 17(a).

5.3.2 Igneous Plutonic Silicates

A similar analysis conducted for the igneous plutonic silicate samples gives the results tabulated in Table 6. Due to the high correlation between iron content and density, density was not selected directly as a significant variate. Figure 17(b) shows the results of regressing ϵ' against a linear equation containing total iron oxide content (Fe₂O₃T), Na₂O, and SiO₂, as parameters. The plutonic results in Table 6

Table 5. Stepwise multivariate regression analysis for ϵ' for igneous volcanic silicate. (N = 20).

	A	B	C	D	E	F	G	H	I
1	Variable Entered	R	R-squared	Y-intercept	Density	SiO ₂ %	TiO ₂ %	Na ₂ O %	MgO %
2									
3	Density	0.8727	0.7616	-1.7876	2.9535				
4	SiO ₂	0.9359	0.8759	3.5161	1.9394	-0.0405			
5	TiO ₂	0.9396	0.8828	3.6676	1.6615	-0.0362	0.4416		
6	Na ₂ O	0.9414	0.8862	4.2352	1.5482	-0.0387	0.4975	-0.0568	
7	MgO	0.9441	0.8914	5.1811	1.7753	-0.0539	0.5579	-0.1782	-0.0817
8	Al ₂ O ₃	0.9459	0.8948						



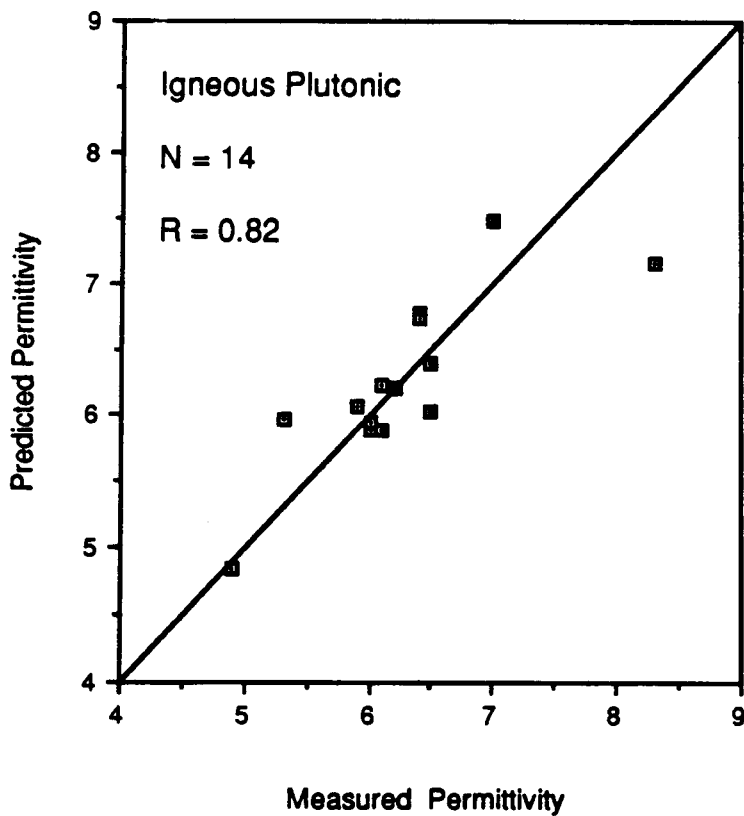
$$\epsilon'_p = 3.5161 + 1.9394 (\text{Density}) - 0.0405 (\text{SiO}_2)$$

(a) Igneous Volcanics

Fig. 17. Computed permittivity versus measured permittivity for (a) igneous volcanics and (b) igneous plutonics.

Table 6. Stepwise multivariate regression analysis for ϵ' for igneous plutonic silicates. (N = 14).

	A	B	C	D	E	F	G	H	I
1	Variable Entered	R	R-squared	Y-intercept	Fe2O3T %	Na2O %	SiO2 %	CaO %	TiO2 %
2									
3	Fe2o3T	0.7287	0.5310	5.2527	0.1393				
4	Na2O	0.7989	0.6382	4.6661	0.1631	0.1186			
5	SiO2	0.8227	0.6769	2.5657	0.2443	0.1753	0.0255		
6	CaO	0.8361	0.6991	3.0145	0.1994	0.1507	0.0188	0.0395	
7	TiO2	0.8827	0.7791	2.8459	0.2276	0.1630	0.0203	0.0960	-0.4544
8	MgO	0.8925	0.7965						
9	MnO	0.9012	0.8122						
10	P2O5	0.9124	0.8325						
11	K2O	0.9260	0.8575						



$$\epsilon'_p = 2.5657 + 0.2443(\text{Fe}_{203\text{T}}) + 0.1753(\text{Na}_2\text{O}) + 0.0255(\text{SiO}_2)$$

(b) Igneous Plutonics

show that the mass percentages of a greater number of cations are significant in determination of ϵ' than was found to be the case for the volcanics in Table 5. This implies that mineralogy plays an important, through possibly secondary role to density, in determining ϵ' .

5.3.3 Igneous Silicates

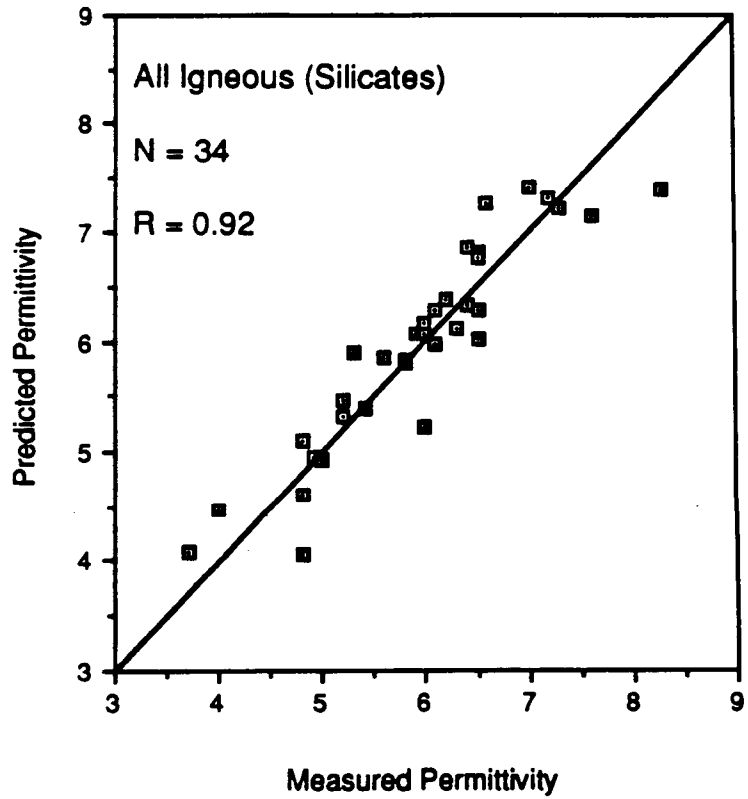
If we combine all 34 igneous silicates into a single class, application of stepwise multivariate regression analysis provides the results given in Table 7 and Fig. 18.

5.3.4 Sedimentary Silicates

For the 20 sedimentary silicate samples, MgO content was selected by the stepwise regression program as the most important variable, followed by SiO_2 , Al_2O_3 , TiO_2 , and density. Results of the regression analysis are given in Table 8 and Fig. 19. Table 8a and Fig. 19a shows the results obtained when density and oxides are included in the analysis. These results are changed dramatically by inclusion of LOI (loss on ignition to $1,000^\circ C$) in the analysis as shown by Table 8b and Fig. 19b. Loss on ignition is related to the vaporization of volatiles, including chemically bound water, during sample preparation for x-ray fluorescence studies. It is probable that the large amount of variance in ϵ' explained by LOI (56%) for the sedimentary silicates is related to the presence of chemically bound water in the sediments. It is interesting to note that inclusion of LOI in the analyses of ϵ' for the igneous silicates did not statistically alter the results.

stepwise multivariate regression analysis for ϵ' for all igneous silicates. (N = 34).

	A	B	C	D	E	F	G	H	I
1	Variable Entered	R	R-squared	Y-intercept	Fe2O3T %	Density	MgO %	TiO2 %	SiO2 %
2									
3	Fe2O3T	0.8087	0.6540	4.8762	0.1952				
4	Density	0.8543	0.7298	1.4511	0.1113	1.4639			
5	MgO	0.8890	0.7904	0.5163	0.1327	1.8415	-0.0376		
6	TiO2	0.9017	0.8131	0.0654	0.1736	2.0560	-0.0498	-0.3876	
7	SiO2	0.9191	0.8447	2.0387	0.1154	2.0947	-0.0591	-0.4703	-0.0259
8	MnO	0.9235	0.8528						
9	P2O5	0.9272	0.8597						
10	CaO	0.9291	0.8632						



$$\epsilon_p = 2.0387 + 0.1154(\text{Fe}_{203\text{T}}) + 2.0947(\text{Density}) - 0.0591(\text{Mg O})$$

Fig. 18. Computed permittivity versus measured permittivity for all igneous silicates combined.

Table 8a.

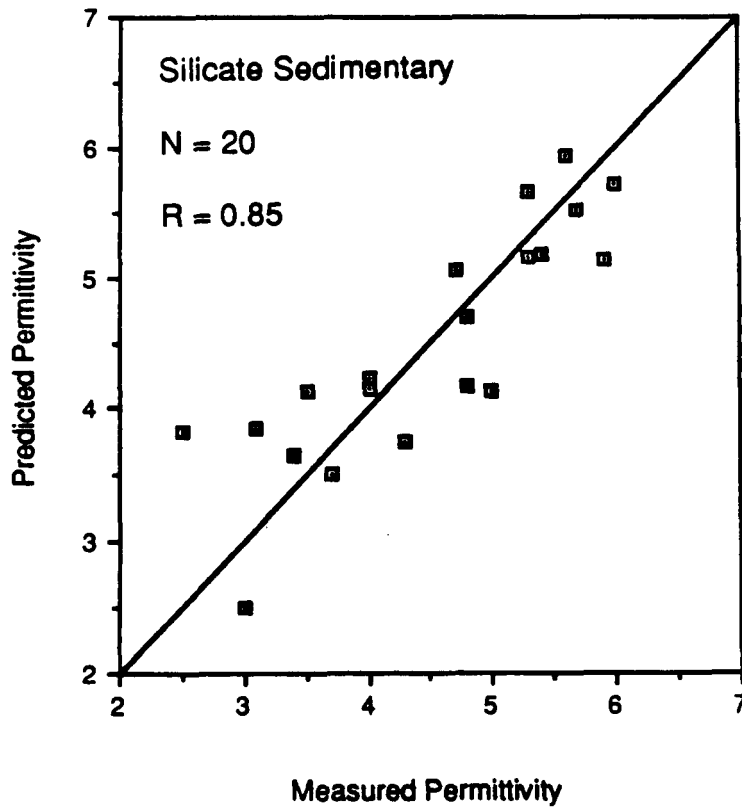
Stepwise multivariate regression analysis for ϵ' for silicate, sedimentary, rocks (a) does not include LOI (loss on ignition) in analysis, and (b) includes LOI in analysis. (N = 20).

(a) does not include LOI (loss on ignition) in analysis.

	A	B	C	D	E	F	G	H	I
1	Variable Entered	R	R-squared	Y-intercept	MgO %	SiO ₂ %	Al ₂ O ₃ %	TiO ₂ %	Density
2									
3	MgO	0.5878	0.3455	3.9982	2.3061				
4	SiO ₂	0.6860	0.4706	7.4257	1.7173	-0.0390			
5	Al ₂ O ₃	0.7845	0.6155	6.4925	1.0863	-0.0456	0.2221		
6	TiO ₂	0.8527	0.7271	6.2882	1.6235	-0.0461	0.3820	-2.2819	
7	Density	0.8705	0.7577	2.1029	1.3692	-0.0396	0.2887	-2.3604	1.6678
8	P2O ₅	0.8734	0.7628						
9	Fe ₂ O ₃ T	0.8748	0.7652						

(b) Includes LOI in analysis.

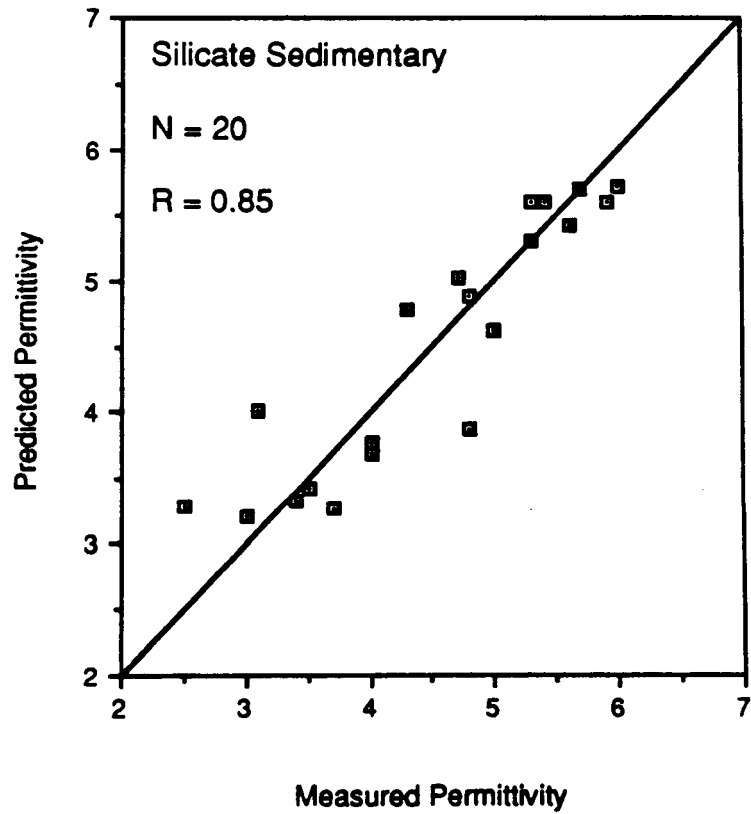
	A	B	C	D	E	F	G	H	I
1	Variable Entered	R	R-squared	Y-intercept	LOI %	CaO %	Na2O %	Density	K2O %
2									
3	LOI	0.7499	0.5623	3.2468	0.2724				
4	CaO	0.8466	0.7168	3.0228	0.3782	-0.1434			
5	Na2O	0.8871	0.7870	2.7080	0.3710	-0.1483	0.4112		
6	Density	0.9127	0.8331	-1.7925	0.3173	-0.1524	0.4442	2.0452	
7	K2O	0.9442	0.8915	-4.5858	0.3182	-0.1769	0.5215	3.0334	0.3579
8	Al2O3	0.9472	0.8972						
9	MnO	0.9505	0.9034						
10	P2O5	0.9552	0.9123						
11	MgO	0.9580	0.9178						
12	Fe2O3T	0.9590	0.9196						



$$\epsilon'_p = 6.2882 + 1.6235(\text{MgO}) - 0.0461(\text{SiO}_2) + 0.3820(\text{Al}_2\text{O}_3) - 2.2819(\text{TiO}_2)$$

(a) Without including LOI (loss on ignition) in analysis

Fig. 19. Computed permittivity versus measured permittivity for sedimentary silicates (a) without including LOI (loss on ignition) in analysis and (b) including LOI in analysis.



$$\epsilon'_p = -1.7925 + 0.3173(\text{LOI}) - 0.1224(\text{CaO}) + 0.4442(\text{Na}_2\text{O}) + 2.0452(\text{density})$$

(b) Including LOI in analysis

5.3.5 All Silicates

Of the total of 54 silicate samples, 34 were igneous and 20 were sedimentary. The combined analysis in Table 9a shows density, aluminum and iron content to be the most significant variates. Not surprisingly, a significant portion of the variance within each of the silicate subgroups is explained by one or more of these variates. Figure 20 shows a plot of a linear regression equation relating ϵ' to density and bulk chemical properties for the silicate samples. It is apparent that ϵ' is dominated by the density of the rock and is secondarily influenced by the chemistry of the sample as a consequence of its mineralogy. Inclusion of LOI in this analysis does not significantly alter these results as shown by Table 9b.

6. ANALYSIS OF DIELECTRIC-LOSS DATA

6.1 Frequency Variation

The dielectric loss factor ϵ'' was measured for 72 rock samples at five frequencies extending between 1.6 GHz and 16 GHz. Figure 21(a) shows plots of ϵ'' versus frequency for four rock groups. Each data point represents the average value of ϵ'' at that frequency for all rock samples belonging to that group. An overall-average plot for all 72 samples is shown in Fig. 21(b). The plots in Fig. 21 indicate that ϵ'' decreases with increasing frequency between 1.6 GHz and 5 GHz and then it levels off at higher frequencies. Among the rock groups shown, the carbonates exhibit the lowest loss and the igneous volcanics exhibit the highest loss.

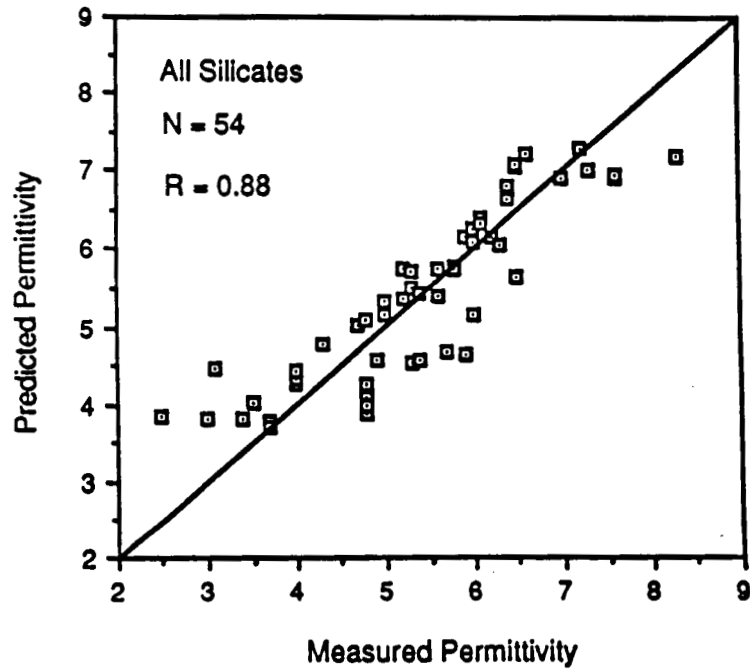
Table 9. Stepwise multivariate regression analysis for ϵ' for all silicate rocks (a) analysis excludes LOI, and (b) analysis includes LOI. (N = 54).

(a) analysis excludes LOI.

	A	B	C	D	E	F	G	H	I
1	Variable Entered	R	R-squared	Y - Intercept	Density	Al ₂ O ₃ %	Fe ₂ O ₃ T %	CaO %	TiO ₂ %
2									
3	Density	0.8304	0.6455	-2.8038	3.2509				
4	Al ₂ O ₃	0.8509	0.7240	-2.5861	2.8500	0.0673			
5	Fe ₂ O ₃ T	0.8751	0.7658	-1.8669	2.4524	0.0727	0.0423		
6	CaO	0.8785	0.7717	-1.3747	2.2356	0.0692	0.0411	0.0294	
7	TiO ₂	0.8846	0.7825	-1.9468	2.4689	0.0786	0.0438	0.0441	-0.3575
8	MnO	0.8865	0.7860						
9	MgO	0.8886	0.7896						
10	P ₂ O ₅	0.8894	0.7910						

(D) analysis includes LOI.

	A	B	C	D	E	F	G	H	I
1	Variable Entered	R	R-squared	Y-intercept	Density	Al2O3 %	LOI %	Fe2O3T %	TiO2 %
2									
3	Density	0.8182	0.6695	-3.6821	3.5601				
4	Al2O3	0.8533	0.7280	-2.9153	2.9865	0.0666			
5	LOI	0.8892	0.7907	-4.1623	3.2428	0.0805	0.1394		
6	Fe2O3T	0.8988	0.8078	-3.4363	2.9164	0.0824	0.1147	0.0271	
7	TiO2	0.9053	0.8196	-4.2427	3.2469	0.0955	0.1140	0.0299	-0.3488
8	P2O5	0.9126	0.8328						
9	SiO2	0.9175	0.8418						
10	MnO	0.9231	0.8521						
11	Na2O	0.9263	0.8581						



$$\epsilon'_p = -1.9468 + 2.4689(\text{Density}) + 0.0786(\text{Al}_2\text{O}_3) + 0.0438(\text{Fe}_2\text{O}_3\text{T}) + 0.0441(\text{CaO}) - 0.3575(\text{TiO}_2)$$

Fig. 20. Predicted versus measured permittivity for all silicate rocks.

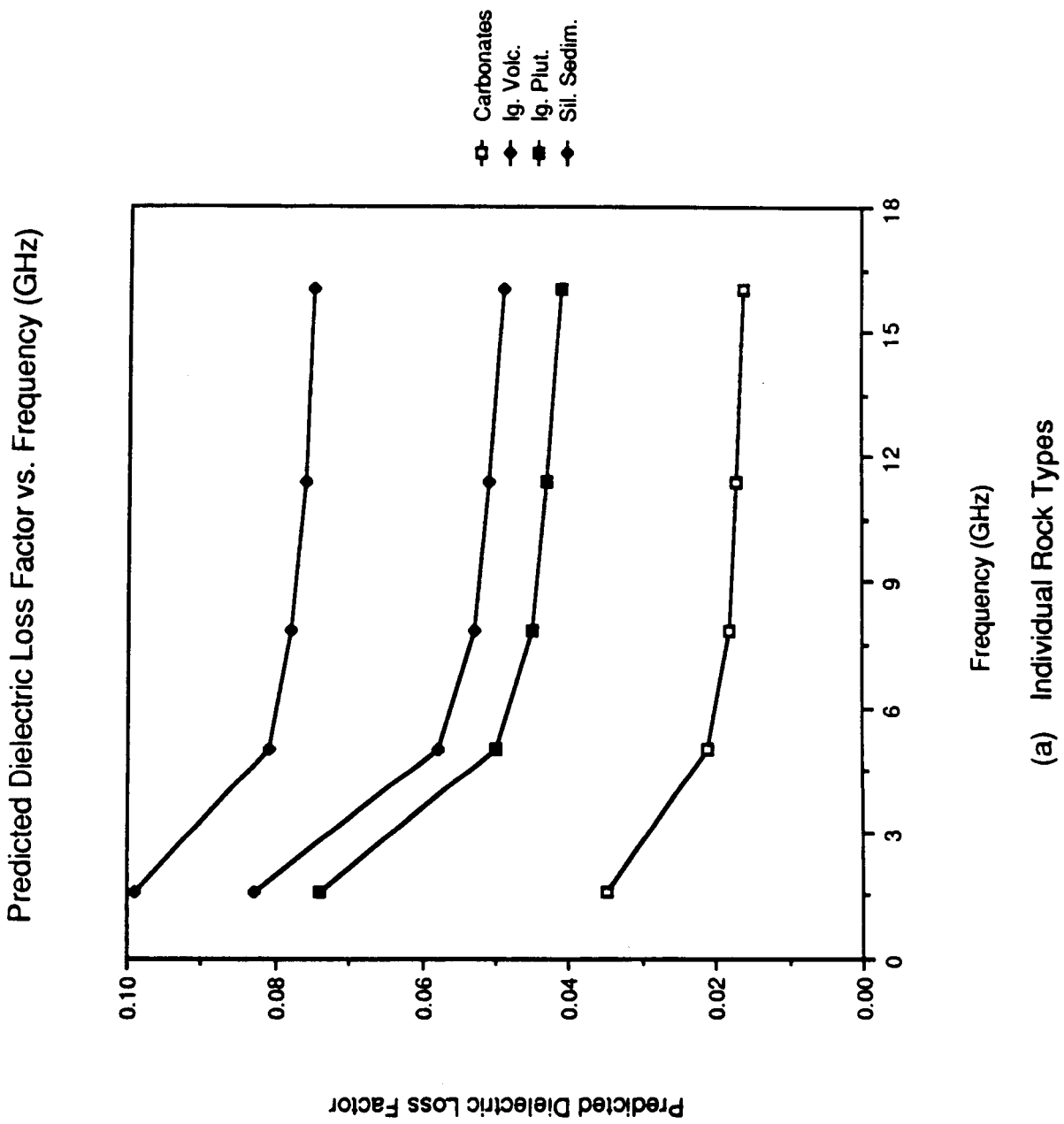
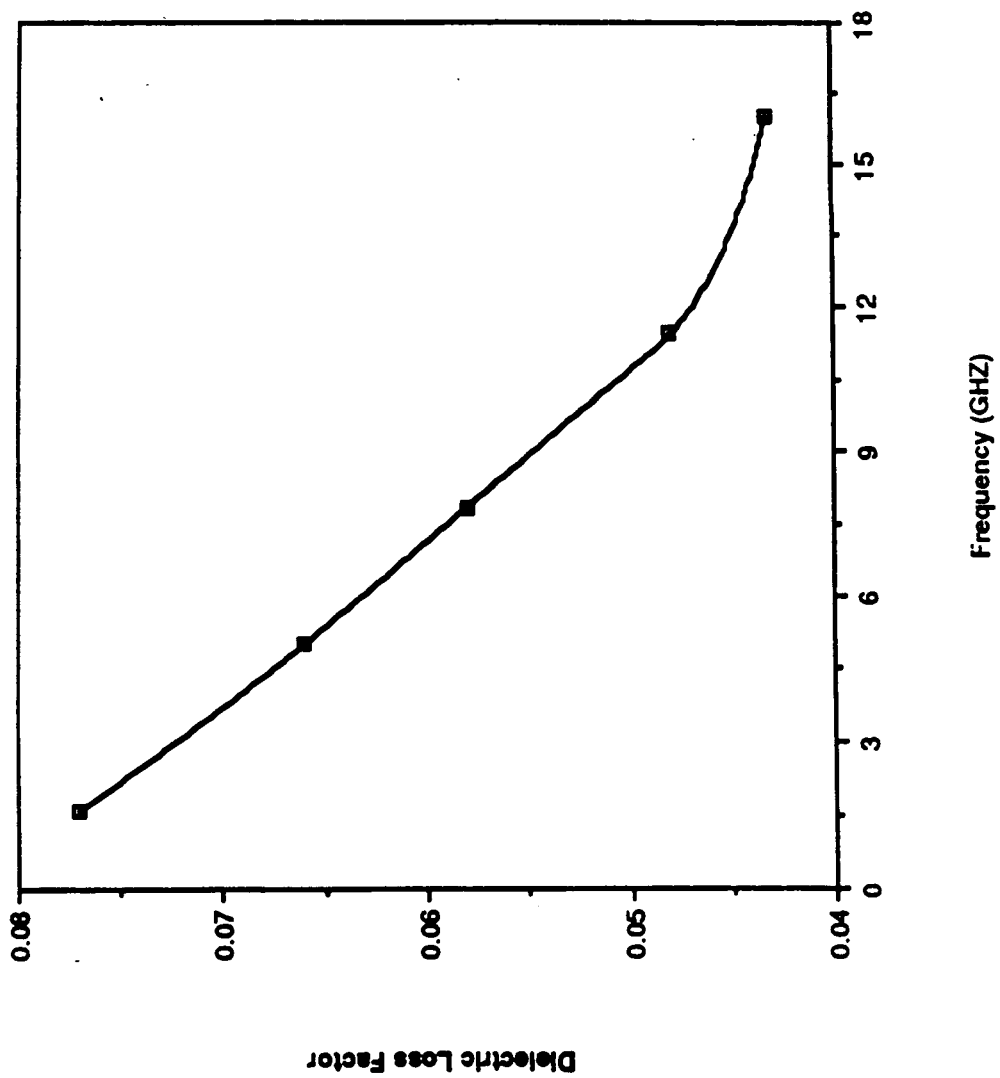


Fig. 21. Spectral variation of ϵ'' for (a) individual rock types and (b) the average for all rock samples.

Dielectric Loss Factor (72 pts.) vs. Frequency (GHz)



(b) Average for all Rock Samples

The loss factor ϵ'' may be modeled as the sum of a conductive component ϵ''_c and a frequency-independent residual component ϵ''_r ,

$$\begin{aligned}\epsilon''(f) &= \epsilon''_r + \epsilon''_c(f) \\ &= \epsilon''_r + \frac{\sigma}{2\pi f \epsilon_0} \\ &\triangleq P_1 + P_2/f\end{aligned}\tag{32}$$

where σ is the conductivity, and P_1 and P_2 are abbreviations for ϵ''_r and $\sigma/2\pi\epsilon_0$, respectively. For each of the measured samples, the values of P_1 and P_2 were determined by fitting the measured data to a linear function of the form given by (32). The frequency was expressed in GHz, which makes P_2 have units of GHz⁻¹.

Figure 22 presents the data measured at 1.6 GHz and 16 GHz in bar-chart format, arranged according to the magnitude of ϵ'' at 1.6 GHz, starting with the largest at the bottom of the left-hand chart and ending with the smallest value at the top of the right-hand chart. Note that the scale is different for the two charts. At 1.6 GHz, the magnitude of ϵ'' extends between a high of 0.24 and a low of less than 0.002.

The constant P_2 of a given sample is proportional to its conductivity σ . The values of P_1 and P_2 determined by the 72 rock samples are arranged in bar-chart format in Fig. 23 according to the magnitude of P_2 .

ORIGINAL PAGE IS
OF POOR QUALITY.

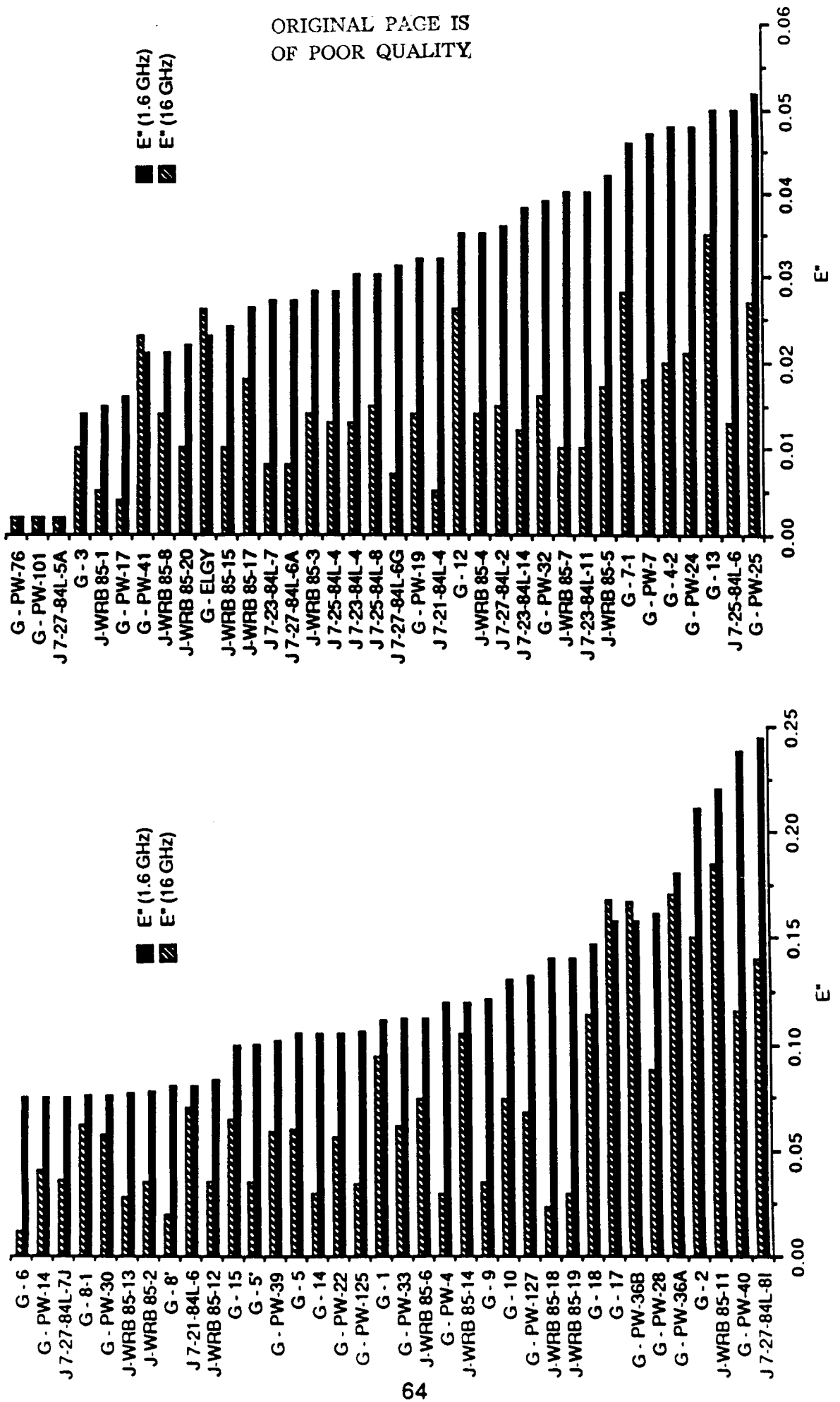


Fig 22 Measured dielectric loss factor at 1.6 GHz and 16 GHz. Note that the

ORIGINAL PAGE IS
OF POOR QUALITY

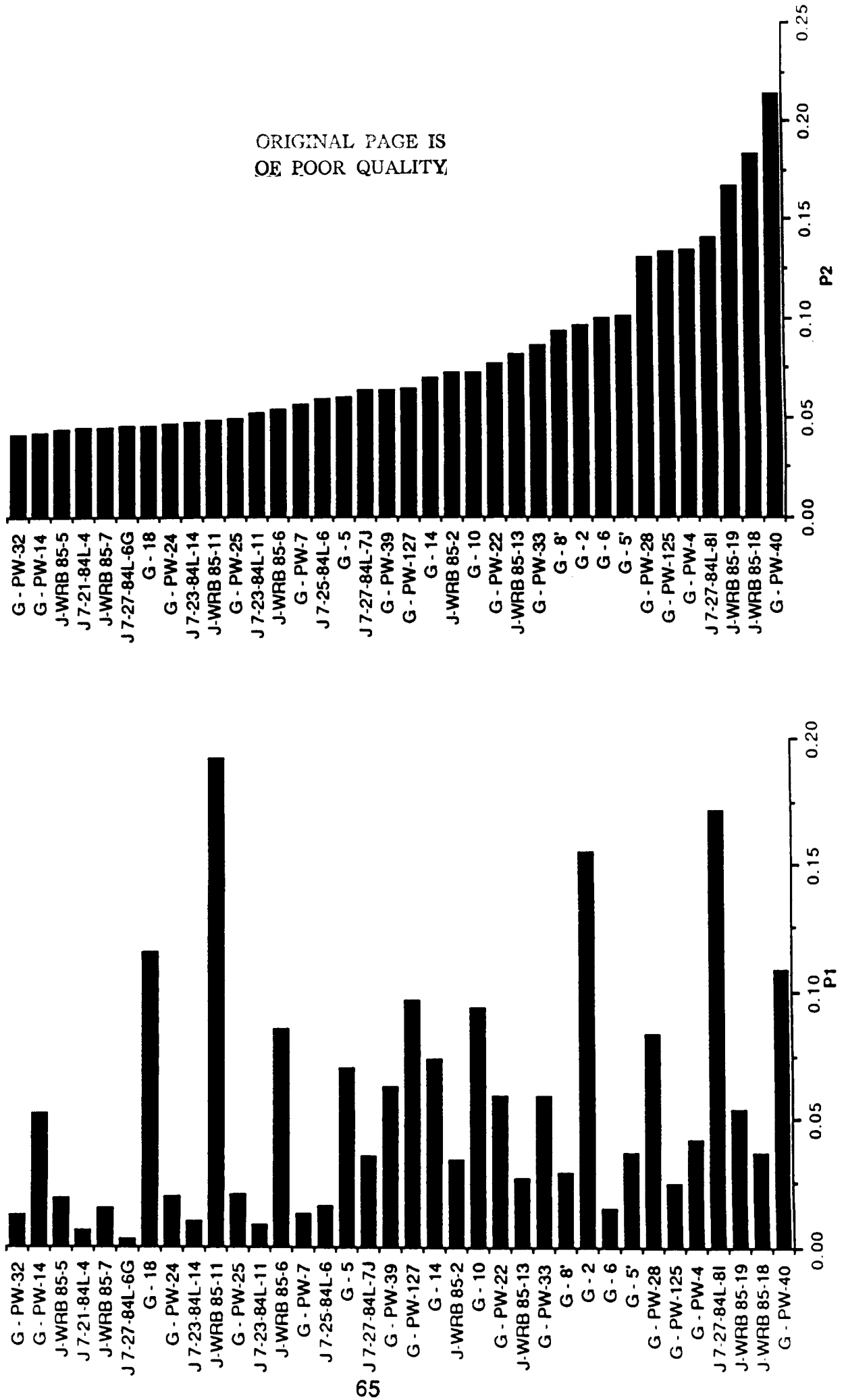


Fig. 23. Bar chart presentation of the constants P1 and P2.

6.2 Dependence on Density

Unlike ϵ' which exhibits a strong dependence on bulk density, the loss factor ϵ'' does not appear to be correlated with ρ (Fig. 24). The same conclusion applies to P_1 and P_2 (Fig. 25).

6.3 Dependence on Mineral Composition

Because ϵ'' is a function of frequency, it was decided to apply the stepwise linear regression analysis on P_1 and P_2 individually, rather than on ϵ'' . The results are tabulated in Tables 10-14 and in Figs. 26-30. Among the 11 variables examined, Fe_2O_3 was found to be the most important single variate for the igneous rocks (Table 12), but that was not the case for the sedimentary rocks (Table 13).

7. CONCLUSIONS

The analysis of microwave dielectric measurements conducted for 80 rock samples has led to the following conclusions:

- (1) The permittivity ϵ' is frequency-independent over the 0.5-18 GHz range.
- (2) The dielectric loss factor ϵ'' exhibits a frequency dependence of the form $\epsilon'' = P_1 + P_2 / f$. For most samples, the second term is significant for $f < 5$ GHz, and may be ignored above 5 GHz.

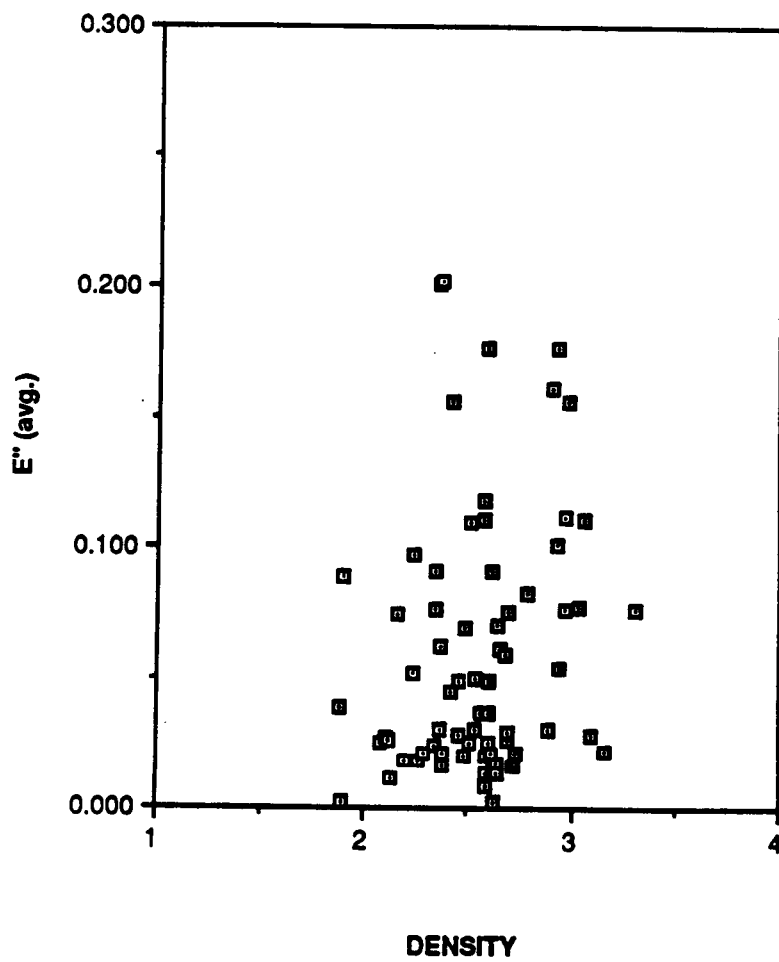


Fig. 24. Dielectric loss factor at 1.6 GHz versus bulk density.

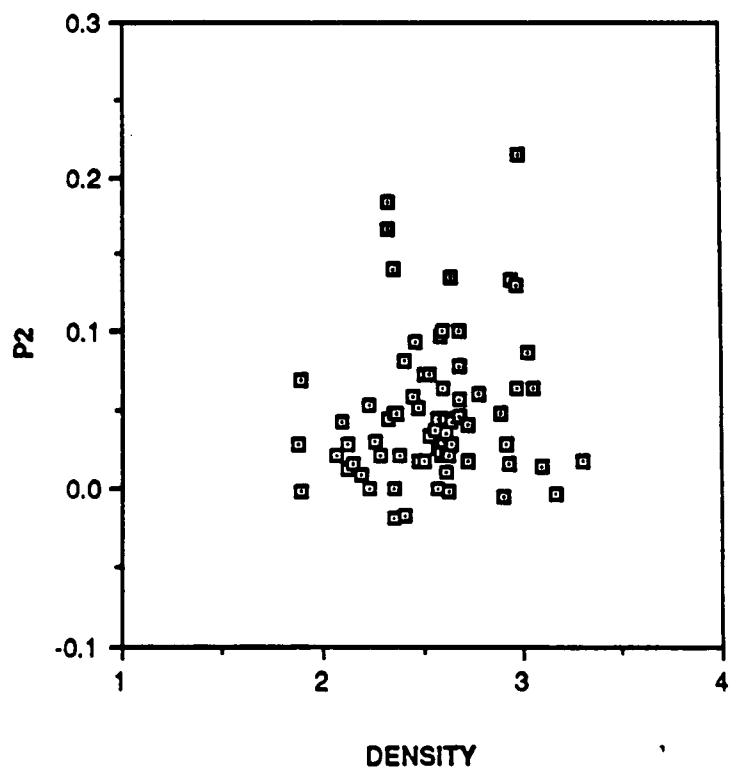
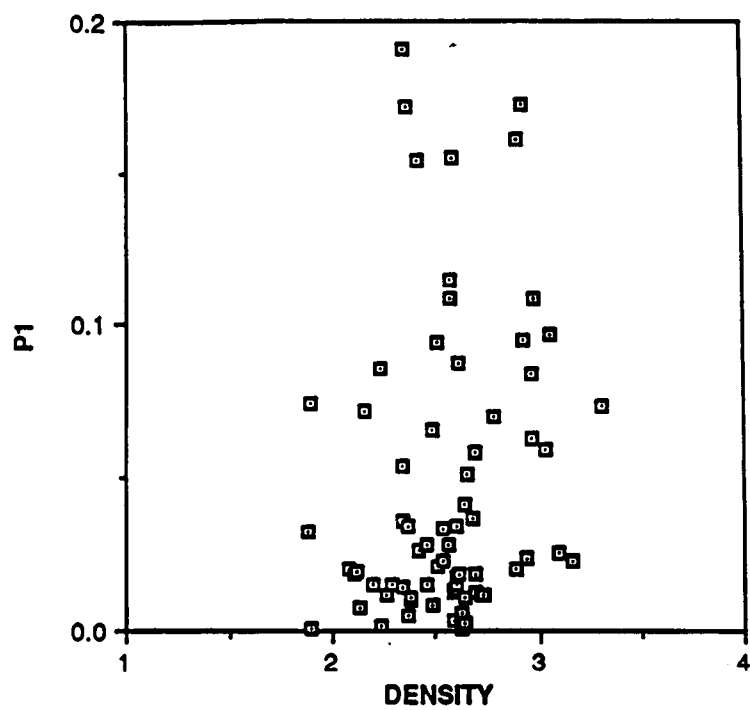
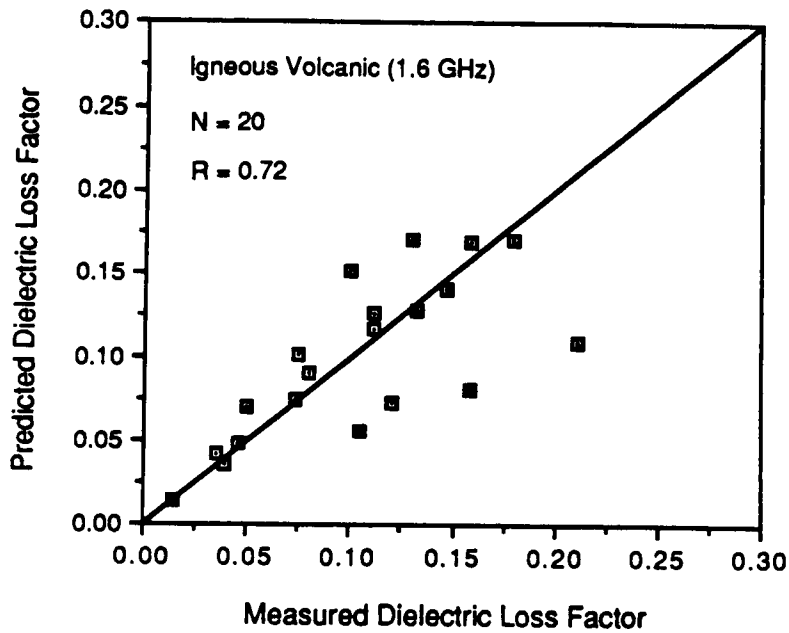
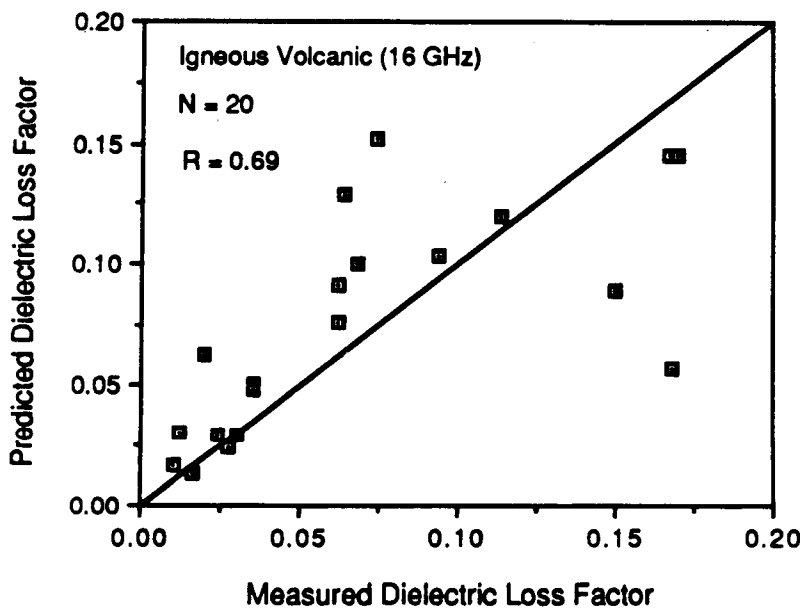


Fig. 25. The constants P_1 and P_2 versus bulk density.



(a) 1.6 GHz



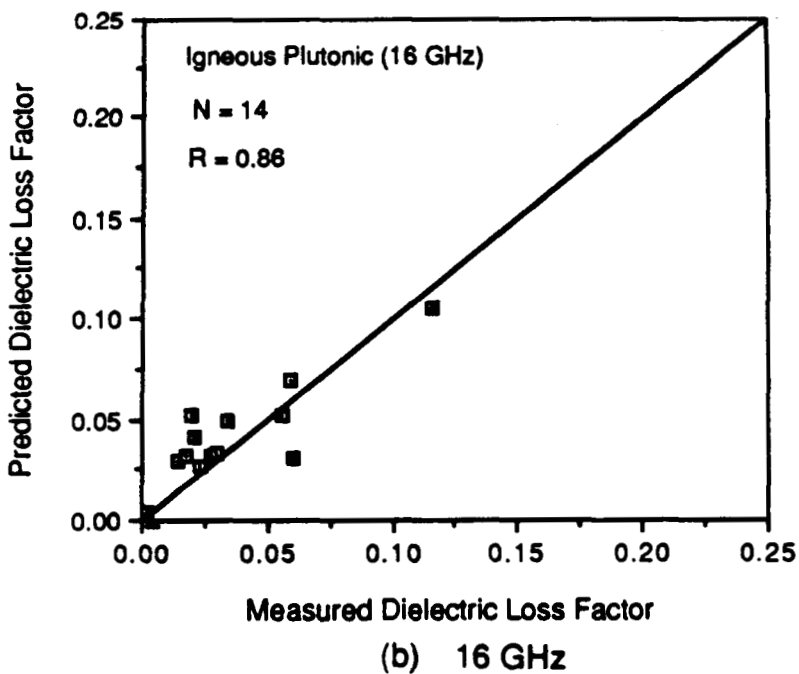
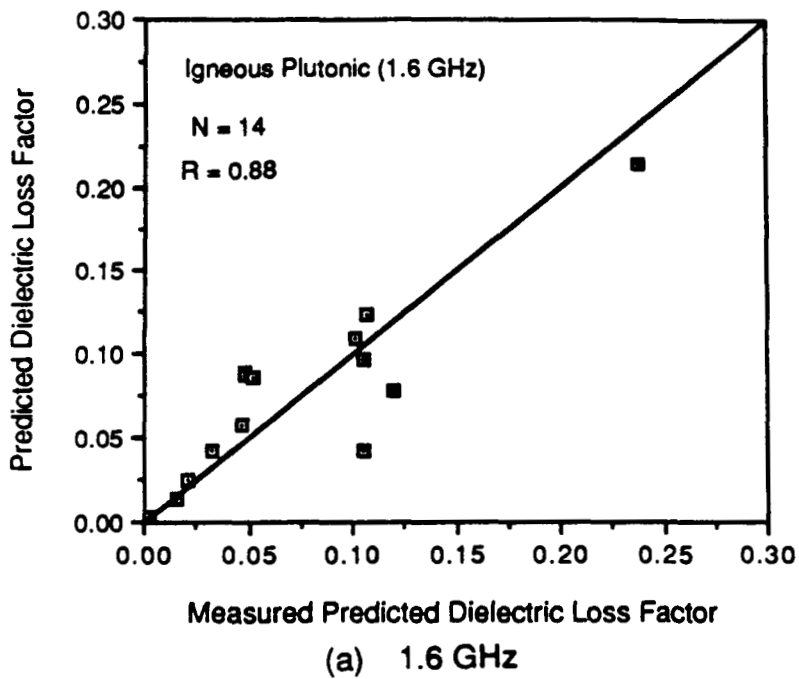
(b) 16 GHz

$$\epsilon_p^* = P_1 + P_2 / f$$

$$P_1 = 0.0341 + 0.0302(\text{Fe}_2\text{O}_3\text{T}) - 0.0118(\text{MgO}) - 0.0090(\text{CaO}) \\ - 0.2523(\text{MnO})$$

$$P_2 = -0.0689 + 0.003(\text{A}12\text{oe}) - 0.0117(\text{Na}_2\text{O}) + 0.0054(\text{K}_2\text{O}) \\ + 0.0297(\text{Density})$$

Fig. 26. Predicted versus measured dielectric loss factor of igneous volcanic rocks.

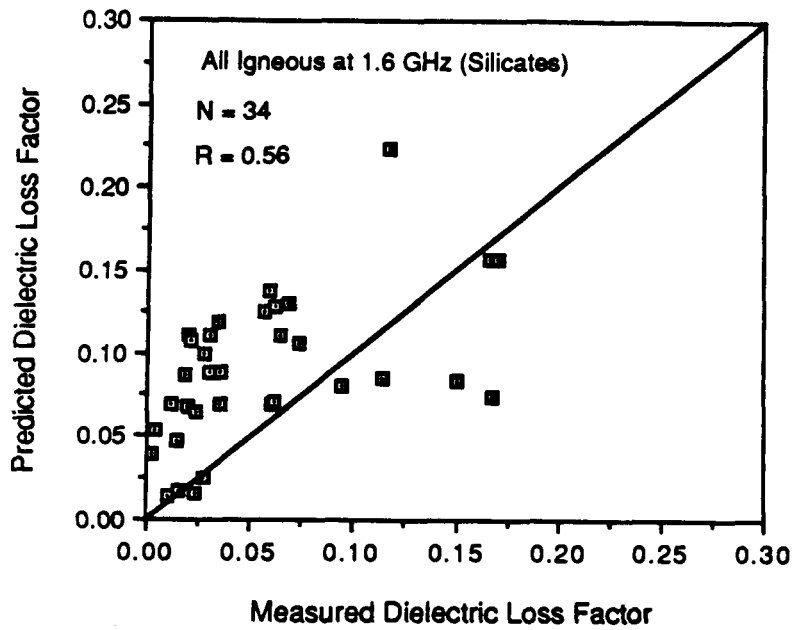


$$\epsilon'' = P_1 + P_2 / f$$

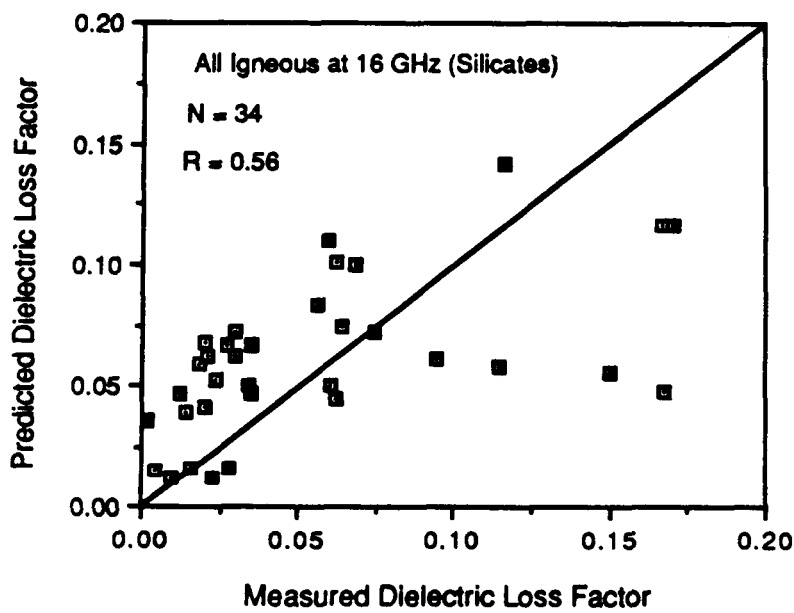
$$P_1 = 0.4559 + 0.223(\text{MnO}) - 0.1724(\text{Density}) + 0.0114(\text{Fe}_2\text{O}_3\text{T}) - 0.0015(\text{Al}_2\text{O}_3)$$

$$P_2 = 0.4685 + 0.0208(\text{Fe}_2\text{O}_3\text{T}) - 0.1789(\text{Density}) - 0.1734(\text{P}_2\text{O}_5) - 0.0024(\text{MgO})$$

Fig. 27. Predicted versus measured dielectric loss factor of igneous plutonic rocks.



(a) 1.6 GHz



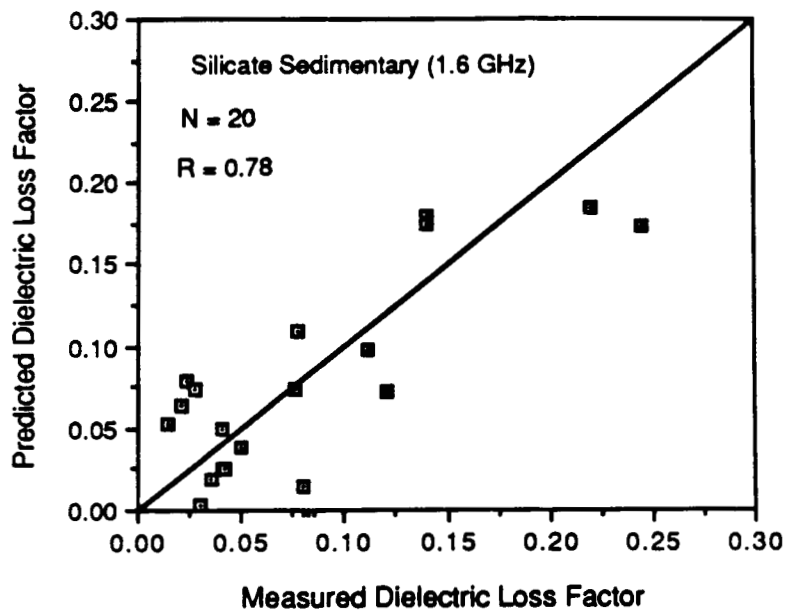
(b) 16 GHz

$$\epsilon'' = P_1 + P_2 / f$$

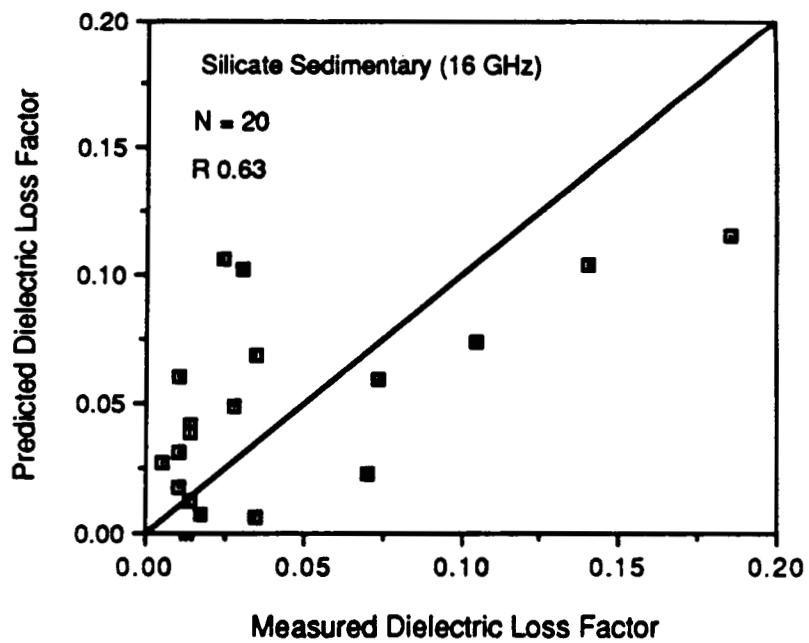
$$P_1 = 0.138 + 0.0187(\text{Al}_2\text{O}_3) - 0.0216(\text{K}_2\text{O}) - 0.1169(\text{TiO}_2) \\ - 0.0014(\text{SiO}_2) - 0.0230(\text{Density})$$

$$P_2 = -0.062 + 0.0392(\text{Na}_2\text{O}) - 0.0166(\text{K}_2\text{O}) - 0.2706(\text{P}_2\text{O}_5) \\ + 0.0028(\text{Fe}_2\text{O}_3\text{T})$$

Fig. 28. Predicted versus measured dielectric loss factor for all igneous rocks.



(a) 1.6 GHz



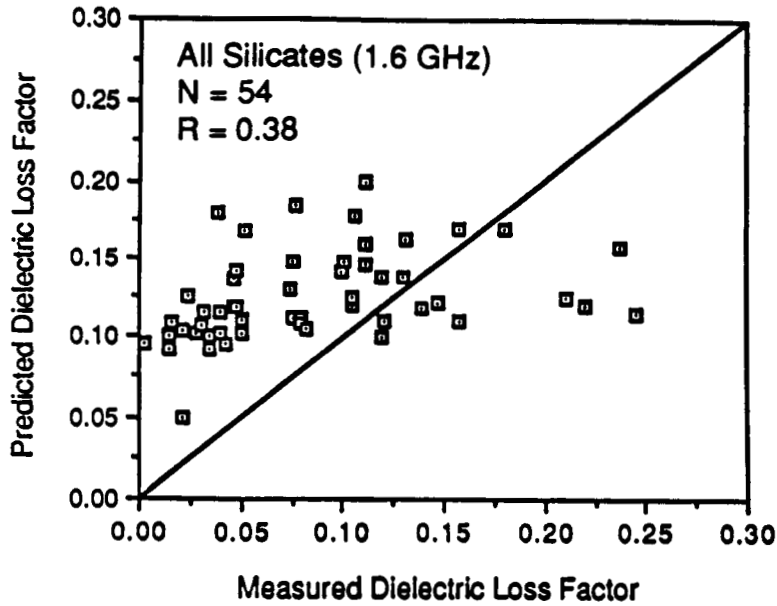
(b) 16 GHz

$$\epsilon'' = P_1 + P_2 / f$$

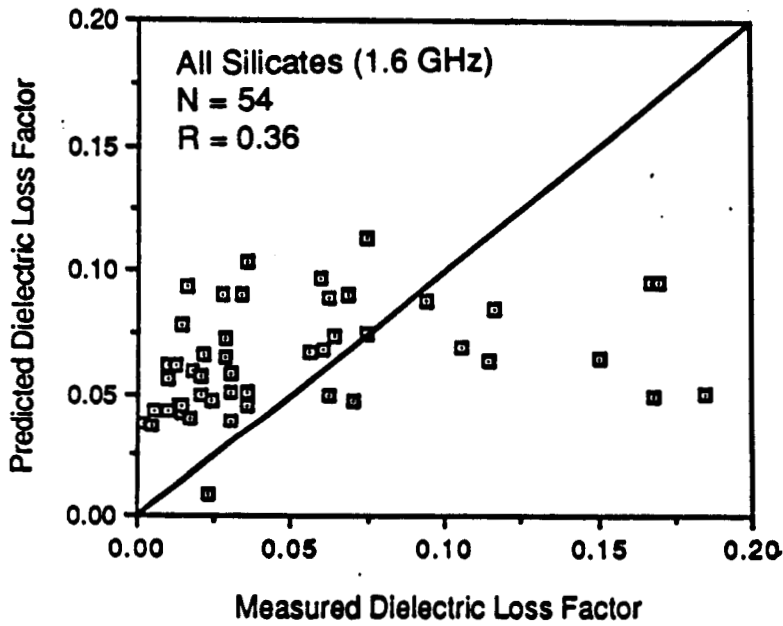
$$P_1 = 0.1385 + 0.0131(\text{Fe}_2\text{O}_3) - 0.0449(\text{Density}) - 0.0023(\text{MgO}) - 0.0301(\text{TiO}_2)$$

$$P_2 = 0.0313 + 0.0154(\text{Fe}_2\text{O}_3) - 0.0082(\text{CaO}) - 0.0037(\text{MgO}) - 0.0712(\text{P}_2\text{O}_5)$$

Fig. 29. Predicted versus measured dielectric loss factor for sedimentary silicates.



(a) 1.6 GHz



(b) 16 GHz

$$\epsilon'' = P_1 + P_2 / f$$

$$P_1 = 0.2224 - 0.0019(\text{SiO}_2) - 0.0040(\text{K}_2\text{O}) - 0.0026(\text{MgO}) - 0.0062(\text{Na}_2\text{O}) - 0.0180(\text{MnO})$$

$$P_2 = -0.0381 + 0.0027(\text{Fe}_{203\text{T}}) - 0.0772(\text{P}_2\text{O}_5) + 0.0037(\text{Al}_{203}) - (0.0053) + 0.0007(\text{AlO}_2)$$

Fig. 30. Predicted versus measured dielectric loss factor for all silicate rocks.

Table 10. Stepwise multivariate regression analysis for ϵ'' for igneous volcanic silicates. (N = 20).

	A	B	C	D	E	F	G	H	I
1					P1				
2	Variable Entered	R	R-squared	Y-intercept	Fe2O3T %	MgO %	CaO %	MnO %	TiO2 %
3									
4	Fe2O3T	0.6385	0.4077	0.0348	0.0088				
5	MgO	0.7234	0.5234	0.0267	0.0189	-0.0126			
6	CaO	0.7789	0.6066	0.0286	0.0269	-0.0121	-0.0086		
7	MnO	0.7834	0.6137	0.0341	0.0302	-0.0118	-0.0090	-0.2523	
8	TiO2	0.8068	0.6509	0.0740	0.0487	-0.0144	-0.0086	-1.0767	-0.0880
9	Na2O	0.8208	0.6737						
10									
11					P2				
12	Variable Entered	R	R-squared	Y-intercept	Al2O3 %	Na2O %	K2O %	Density	
13									
14	Al2O3	0.2113	0.0446	0.0146	0.0018				
15	Na2O	0.3765	0.1417	0.0137	0.0037	-0.0110			
16	K2O	0.3847	0.1480	0.0109	0.0037	-0.0114	0.0014		
17	Density	0.4161	0.1731	-0.0689	0.0033	-0.0117	0.0054	0.0297	

Table 11. Stepwise multivariate regression analysis for ϵ'' for igneous plutonic silicates. (N = 14).

	A	B	C	D	E	F	G	H	I
1									
2	Variable Entered	R	R-squared	Y-intercept	P1 MnO %	Density	Fe2O3T %	Al2O3 %	Na2O %
3									
4	MnO	0.6435	0.4141	0.0039	0.2949				
5	Density	0.6958	0.4841	0.1540	0.4241	-0.0584			
6	Fe2O3T	0.7907	0.6252	0.3039	0.1360	-0.1201	0.0075		
7	Al2O3	0.8245	0.6797	0.4559	0.0223	-0.1724	0.0114	-0.0015	
8	Na2O	0.8826	0.7790	0.6508	-0.2761	-0.2482	0.0214	-0.0059	0.0112
9	P2O5	0.9252	0.8560						
10	K2O	0.9267	0.8588						
11					P2				
12	Variable Entered	R	R-squared	Y-intercept	Fe2O3T %	Density	P2O5 %	MgO %	CaO %
13									
14	Fe2O3T	0.4690	0.2199	0.0150	0.0069				
15	Density	0.7287	0.5311	0.7944	0.0193	-0.3094			
16	P2O5	0.8431	0.7109	0.8650	0.0228	-0.3350	-0.1296		
17	MgO	0.8859	0.7848	0.4685	0.0208	-0.1789	-0.1734	-0.0024	
18	CaO	0.9333	0.8711	-0.4248	0.0235	0.1653	-0.0735	-0.0071	-0.0163
19	TiO2	0.9458	0.8945						
20	MnO	0.9585	0.9187						
21	K2O	0.9695	0.9399						
22	SiO2	0.9781	0.9566						

Table 12. Stepwise multivariate regression analysis for ϵ'' for all igneous silicate samples. (N = 20).

	A	B	C	D	E	F	G	H	I
1					P1				
2	Variable Entered	R	R-squared	Y-intercept	Fe2O3T %	Density	MgO %	TiO2 %	Na2O %
3									
4	Fe2O3T	0.4089	0.1672	0.0313	0.0048				
5	Density	0.5017	0.2517	0.2079	0.0092	-0.0755			
6	MgO	0.5348	0.2861	0.1736	0.0099	-0.0616	-0.0014		
7	TiO2	0.5861	0.3435	0.1385	0.0131	-0.0449	-0.0023	-0.0301	
8	Na2O	0.6040	0.3648	0.1361	0.0131	-0.0382	-0.0028	-0.0301	-0.0044
9	MnO	0.6180	0.3819						
10	P2O5	0.6310	0.3982						
11	SiO2	0.6337	0.4016						
12	Al2O3	0.6431	0.4136						
13									
14					P2				
15	Variable Entered	R	R-squared	Y-intercept	Fe2O3T %	CaO %	MgO %	P2O5 %	Al2O3 %
16									
17	Fe2O3T	0.3268	0.1068	0.0298	0.0037				
18	CaO	0.4116	0.1694	0.0306	0.0071	-0.0044			
19	MgO	0.5851	0.3423	0.0269	0.0144	-0.0088	-0.0034		
20	P2O5	0.6226	0.3877	0.0313	0.0154	-0.0082	-0.0037	-0.0712	
21	Al2O3	0.6490	0.4212	0.0042	0.0150	-0.0088	-0.0031	-0.0754	0.0020
22	Na2O	0.6721	0.4517						
23	Density	0.6765	0.4576						
24	K2O	0.6804	0.4630						

Table 13. Stepwise multivariate regression analysis for ϵ'' for sedimentary silicates. (N = 34).

	A	B	C	D	E	F	G	H	I
1					P1				
2	Variable Entered	R	R-squared	Y-intercept	Al2O3 %	Na2O %	Fe2O3T %	K2O %	TiO2 %
3									
4	Al2O3	0.5552	0.3083	-0.0680	0.0155				
5	Na2O	0.6154	0.3787	-0.0736	0.0137	0.0216			
6	Fe2O3T	0.6644	0.4414	-0.0872	0.0142	0.0250	0.0014		
7	K2O	0.6968	0.4855	-0.0635	0.0139	0.0227	0.0014	-0.0142	
8	TiO2	0.7120	0.5069	-0.0669	0.0177	0.0129	0.0014	-0.0155	-0.0617
9	MgO	0.7724	0.5966						
10	Density	0.8065	0.6505						
11	MnO	0.8166	0.6668						
12	SiO2	0.8187	0.6702						
13									
14					P2				
15	Variable Entered	R	R-squared	Y-intercept	Na2O %	K2O %	Al2O3 %	MnO %	MgO %
16									
17	Na2O	0.5749	0.3305	0.0142	0.0444				
18	K2O	0.7291	0.5316	0.0587	0.0394	-0.0297			
19	Al2O3	0.7502	0.5628	0.0242	0.0362	-0.0291	0.0050		
20	MnO	0.7733	0.5980	0.0119	0.0374	-0.0292	0.0060	0.0139	
21	MgO	0.8042	0.6468	-0.0002	0.0403	-0.0277	0.0083	0.0176	-0.0479
22	CaO	0.8090	0.6544						
23	P2O5	0.8114	0.6583						
24	Fe2O3T	0.8139	0.6624						

Table 14. Stepwise multivariate regression analysis for ϵ'' for all silicate samples. (N = 54).

	A	B	C	D	E	F	G	H	I
1									
2	Variable Entered	R	R-squared	Y - Intercept	P1 SiO2 %	K2O %	MgO %	Na2O %	MnO %
3									
4	SiO2	0.2529	0.0640	0.1099	-0.0008				
5	K2O	0.2777	0.0771	0.1180	-0.0008	-0.0034			
6	MgO	0.3236	0.1047	0.1569	-0.0012	-0.0054	-0.0016		
7	Na2O	0.3352	0.1124	0.1810	-0.0015	-0.0041	-0.0019	-0.0035	
8	MnO	0.3595	0.1292	0.2224	-0.0019	-0.0040	-0.0026	-0.0062	-0.0180
9	Fe2O3T	0.4275	0.1828						
10	TiO2	0.4868	0.2370						
11	Al2O3	0.4926	0.2426						
12									
13					P2				
14	Variable Entered	R	R-squared	Y - Intercept	Fe2O3T %	P2O5 %	Al2O3 %	K2O %	SiO2 %
15									
16	Fe2O3T	0.1644	0.0270	0.0449	0.0012				
17	P2O5	0.2361	0.0557	0.0505	0.0018	-0.0634			
18	Al2O3	0.3108	0.0966	0.0304	0.0019	-0.0846	0.0019		
19	K2O	0.3452	0.1191	0.0349	0.0016	-0.0817	0.0025	-0.0048	
20	SiO2	0.3684	0.1357	-0.0381	0.0027	-0.0772	0.0037	-0.0053	0.0007
21	MnO	0.4170	0.1739						
22	Na2O	0.4289	0.1839						
23	MgO	0.4371	0.1910						

(3) The bulk density ρ accounts for about 50% of the variance of ϵ' . For individual rock types (by genesis), about 90% of the observed variance of ϵ' may be explained by the combination of density, SiO_2 content, Fe_2O_3 content, MgO content, and TiO_2 content.

(4) The loss factor ϵ'' appears to be statistically uncorrelated with density.

(5) Although multivariate regression equations were generated to relate ϵ'' to bulk sample chemistry, the results are not considered very significant (statistically) because the correlation coefficient between the measured and computed values of ϵ'' is poor.

(6) Additional tests are needed to determine the dependence of ϵ'' on mineral composition.

REFERENCES

1. Campbell, M. J. and J. Ulrichs, "Electrical properties of rocks and their significance for lunar radar observations," *JGR* 74 (1969) 5867-5881.
2. Olhoeft, G. R., A. L. Frisillo, and D. W. Strangway, "Electrical properties of lunar soil sample 15301, 38," *JGR* 79 (1974) 1599-1604.
3. Strangway, D. W., G. R. Olhoeft, W. B. Chapman and J. Carnes, "Electrical properties of lunar soils: dependence upon frequency, temperature and moisture," *Earth Planet Sci. Lett.*, 16 (1972) 275-281.
4. Olhoeft, G. R. and D. W. Strangway, "Dielectric properties of the first 100 meters of the Moon," *Earth Planet Sci. Lett.*, 24 (1975) 394-404.
5. Parkhomenko, E.I., Electrical Properties of Rocks, Plenum Press, New York, 314 pp.
6. von Hippel, A. R., Dielectric Materials and Applications, John Wiley, New York, 405 pp., 1954.
7. Stuchly, M. A., T. W. Athey, G. M. Samaras, and G. E. Taylor, "Measurement of radio frequency permittivity of biological tissues with an open-ended coaxial line: Part II, Experimental results," *IEEE Trans. Microwave Theory Tech.*, vol. MTT-30, No. 1, pp. 87-92, Jan. 1982.
8. Burdette, E. C., F. L. Cain, and J. Seals, "In Vivo probe measurement technique for determining dielectric properties at VHF through microwave frequencies," *IEEE Trans. Microwave Theory Tech.*, vol. MTT-28, no. 4, pp. 414-427, April 1980.
9. Athey, T. W., M. A. Stuchly, and S. S. Stuchly, "Measurement of radio frequency permittivity of biological tissues with an open-ended coaxial line: Part I," *IEEE Trans. Microwave Theory Tech.*, vol. MTT-30, no. 1, pp. 82-86, Jan. 1982.
10. Marcuvitz, N., Waveguide Handbook, New York, Dover, 1965.
11. Deschamps, G. A., "Impedance of antenna in a conducting medium," *IRE Trans. Antennas Propagat.*, pp. 648-650, Sept. 1962.
12. Ulaby, F. T., R. K. Moore, and A. K. Fung, Microwave Remote Sensing, vol. 3. Dedham, MA: Artech, 1986, Appendix E.
13. Jordan, B. P., R. J. Sheppard, and S. Szwarnowski, "The dielectric properties of formamide, ethanediol, and methanol," *J. Phys. D: Appl. Phys.*, vol. 11, 1978.

14. Harrington, Roger F., Time-Harmonic Electromagnetic Fields, New York, McGraw-Hill Book Company, 1961, pp. 317-326.